Neurobiology of Disease 217 (2025) 107182

Contents lists available at ScienceDirect

Neurobiology of Disease

journal homepage: www.elsevier.com/locate/ynbdi

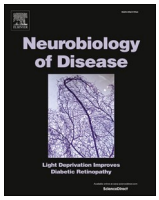

Early alpha-synuclein accumulation, oxidative stress and inflammation in the proximal colon of c-rel$^{-/-}$ mouse model of Parkinson's disease

Edoardo Parrella [a,b,c], Michele Mario Gennari [a], Giulia Abate [a], Mariachiara Pucci [a], Tiziana Schioppa [d], Daniela Bosisio [d], Emanuela Tirelli [a], Marina Benarese [a], Gaia Vegezzi [a], Maria Grazia Silletti [a], Chiara Fritzsch [a], Daniela Uberti [a], Marina Pizzi [a,*], Vanessa Porrini [a]

[a] Department of Molecular and Translational Medicine, Division of Pharmacology, University of Brescia, Italy
[b] Departmental Faculty of Medicine, Saint Camillus International University of Health Sciences, Rome, Italy
[c] Section of Innovation Biomedicine, Department of Engineering for Innovation Medicine, University of Verona, Verona, Italy
[d] Department of Molecular and Translational Medicine, Division of Experimental Oncology and Immunology, University of Brescia, Brescia, Italy

ARTICLE INFO

Keywords:
Parkinson's disease
Intestine
Mouse model
NF-κB/c-Rel
α-synuclein
Inflammation
Oxidative stress

ABSTRACT

A growing body of evidence links the gastrointestinal tract to Parkinson's disease (PD) development. The research by Braak and colleagues, based on analyzing post-mortem samples from PD patients, suggests that the pathology begins in the gut and progresses to the brain. Our recent work shows that PD brains and PD PBMCs display reduced DNA-binding activity of the NF-κB/c-Rel subunit, a neuroprotective transcription factor that promotes brain expression of mitochondrial regulators such as B-cell lymphoma-extra-large (Bcl-xL), uncoupling protein 4 (UCP4), and manganese superoxide dismutase (MnSOD). Previous studies have also shown that male mice lacking the NF-κB/c-Rel subunit (c-rel$^{-/-}$ mice) develop age-related parkinsonian neuropathology linked to both non-motor and motor symptoms. They exhibit a Braak pattern of α-synuclein (α-syn) deposition, beginning with early gut involvement marked by constipation and α-syn accumulation in the distal colon from 2 months old. Here, we further examine the progression of intestinal pathology in the proximal colon of c-rel$^{-/-}$ male mice which is connected to the brain *via* the vagus nerve, using microscopy, biochemistry, and multispectral opto-acoustic tomography. At 2 months, α-syn and phosphorylated α-syn accumulation was detected in the myenteric plexus of c-rel$^{-/-}$ mice, with significantly greater accumulation at 10 months. Intestinal synucleinopathy was accompanied by notable oxidative stress, evidenced by increased NADPH oxidase activity and higher levels of 3-nitrotyrosine-modified proteins in the proximal colon. By 10 months, c-rel$^{-/-}$ mice showed gut inflammation with elevated interleukin-6 expression, infiltration of CD11b+Ly6G+ neutrophils, and increased oxygenated hemoglobin in the proximal colon, along with colon shortening and loss of TH-positive neurons. These findings, in addition to supporting the role of NF-κB/c-Rel dysregulation in PD pathophysiology, show that c-rel$^{-/-}$ mice develop progressive PD-like pathology in the proximal colon and provide an invaluable model for studying the potential gut-to-brain spread of endogenous α-syn *via* the vagus.

1. Introduction

Parkinson's disease (PD) is the most common neurodegenerative movement disorder, with a higher prevalence in men than in women (Wooten et al., 2004; Balestrino and Schapira, 2020; Ben-Shlomo et al., 2024). Main pathological features of PD are the loss of dopaminergic neurons in the substantia nigra pars compacta (SNpc) and the accumulation of α-synuclein (α-syn) (Poewe et al., 2017). This protein is normally expressed as a component of the central and enteric nervous systems (CNS and ENS, respectively) (Böttner et al., 2012; Longhena et al., 2019). However, in pathological conditions α-syn aggregates to form insoluble fibrils that are the main constituents of Lewy bodies (LB)

* Corresponding author.
E-mail addresses: edoardo.parrella@univr.it (E. Parrella), michele.gennari@unibs.it (M.M. Gennari), giulia.abate@unibs.it (G. Abate), mariachiara.pucci@unibs.it (M. Pucci), tiziana.schioppa@unicamillus.org (T. Schioppa), daniela.bosisio@unibs.it (D. Bosisio), e.tirelli004@unibs.it (E. Tirelli), marina.benarese@unibs.it (M. Benarese), gaia.vegezzi@libero.it (G. Vegezzi), mariagrazia.silletti@studenti.univr.it (M.G. Silletti), chiara.fritzsch@unibs.it (C. Fritzsch), daniela.uberti@unibs.it (D. Uberti), marina.pizzi@unibs.it (M. Pizzi), vanessa.porrini@unibs.it (V. Porrini).

https://doi.org/10.1016/j.nbd.2025.107182
Received 27 June 2025; Received in revised form 17 October 2025; Accepted 6 November 2025
Available online 7 November 2025

and Lewy neurites (LN), proteinaceous inclusions observed in the brain of PD patients. Similarly, α-syn is detected at higher levels, also as LB-like aggregates, in the intestines of PD patients (Aldecoa et al., 2015; Gold et al., 2013; Shannon et al., 2012a; Shannon et al., 2012b; Hilton et al., 2014; Braak et al., 2006; Forsyth et al., 2011; Stokholm et al., 2016; Phillips et al., 2008). Importantly, some studies reported abnormal α-syn accumulation in intestinal biopsies collected from subjects up to 8 years prior to the onset of motor symptoms, indicating enteric α-syn pathology as an early event in PD (Shannon et al., 2012b; Hilton et al., 2014).

In addition to the well-known motor deficits, PD is characterized by several non-motor symptoms that often precede the onset of movement issues, including constipation, hyposmia, anxiety, depression and sleep behavior disorders (Kalia and Lang, 2015). Among these non-motor symptoms, constipation is one of the most common (Chen et al., 2015) and one of the earliest indicators of the pathological processes that ultimately lead to PD, appearing even more than 20 years before disease diagnosis (Savica et al., 2009; Postuma et al., 2013; Abbott et al., 2002).

The early appearance of intestinal dysfunction, together with the abnormal α-syn deposition in the ENS observed before CNS neurodegeneration, have suggested that α-syn pathology may start in the gut and then propagates to the brain (Dogra et al., 2022; Fitzgerald et al., 2019; Perez-Pardo et al., 2017). Based on the topographical pattern of LB deposition, and on the early involvement of structures providing parasympathetic innervation to the gut, Braak and colleagues proposed that α-syn pathology could spread from the ENS to the brain through the vagus nerve (Braak et al., 2003; Hawkes et al., 2007).

Several mechanisms have been proposed to play a role in PD pathogenesis, including oxidative stress, inflammation, mitochondrial deficits, and impaired autophagy (Poewe et al., 2017; Faustini et al., 2017). Interestingly, the family of transcription factors Nuclear Factor-κB (NF-κB) can regulate some of these molecular pathways (Bellucci et al., 2020; Lanzillotta et al., 2015). NF-κB consists of five different subunits (p65/RelA, RelB, c-Rel, p50, and p52) that combine to form homo- or heterodimers (Gilmore and Wolenski, 2012; Sarnico et al., 2012). c-Rel subunit within the activated NF-κB dimers exerts a neuroprotective action based on its positive regulation of genes involved in mitochondrial homeostasis, including the B-cell lymphoma-extra-large (Bcl-xL) and the uncoupling protein 4 (UCP4), or in scavenging reactive oxygen species (ROS), such as the manganese superoxide dismutase (MnSOD) (Sarnico et al., 2009). Our recent results, showing a reduction of the DNA-binding activity of NF-κB/c-Rel in the SN and peripheral blood mononuclear cells (PBMCs) from PD patients, suggest a possible pathogenic role for this subunit in PD (Porrini et al., 2023).

In support of this, male mice lacking the NF-κB/c-Rel subunit (c-rel$^{-/-}$ mice), a model of PD-like pathology (Baiguera et al., 2012), show a lower expression of Bcl-xL, UCP4, and MnSOD in the SNpc, which is age-dependent and displays a Braak-like pattern of ascending α-syn deposition (Parrella et al., 2019). Alpha-syn accumulation is detectable in the olfactory bulbs as well as in the dorsal motor nucleus of vagus (DMV) and locus coeruleus (LC) at 5–7 months, while it becomes evident in the SNpc at 12 months (Parrella et al., 2019). At this age, the α-syn pathology is associated with a drop of dopamine transporter (DAT) in the striatum and nigral inflammation (Parrella et al., 2019; Porrini et al., 2017). At 18 months, c-rel$^{-/-}$ mice develop loss of dopaminergic neurons in the SNpc and dopaminergic terminals in the striatum, with accumulation of iron and microglia activation (Baiguera et al., 2012). The pathology progression is accompanied by the appearance of both non-motor and motor symptoms, including hyposmia at 2 months, anxiety- and depressive-like behavior at 12 months with apathy (Parrella et al., 2019; Parrella et al., 2022), and motor deficits responsive to L-DOPA administration at 18 months (Baiguera et al., 2012). We also reported early involvement of the gut in the pathology associated with the c-rel$^{-/-}$ mouse model. Starting at 2 months of age, c-rel$^{-/-}$ male mice show reduced stool frequency and water content, two signs of prolonged colonic transit time and decreased colon motility (Parrella et al., 2019). Interestingly, 2-month-old c-rel$^{-/-}$ male mice exhibit α-syn accumulation in the myenteric plexus of the distal colon (Parrella et al., 2019), which is the gastrointestinal region most involved in intestinal motility (France et al., 2012). Finally, our recent findings revealed sex-related differences in nigro-striatal degeneration and behavior of c-rel$^{-/-}$ mice, with aged c-rel$^{-/-}$ females showing a minor reduction in striatal dopaminergic fibers and not developing significant motor deficits or non-motor symptoms such as constipation, hyposmia, depressive-like and apathetic behaviors, compared to wild-type (wt) littermates (Parrella et al., 2025). The c-rel$^{-/-}$ mouse model is therefore considered a relevant experimental model of sporadic PD, reflecting multiple features of the human disease (Jiang and Dickson, 2018; Dovonou et al., 2023; Lal and Chopra, 2024).

In this study, we demonstrate that the intestinal disease progression, in terms of α-syn accumulation, oxidative stress, and inflammation occurs also in the proximal colon of c-rel$^{-/-}$ male mice, a gut region innervated by the vagus nerve in both rodents and humans (Gonella et al., 1987; Berthoud et al., 1991; Berthoud and Neuhuber, 2000). We aimed to further characterize intestinal alterations in this specific region to support future studies on the potential vagus nerve-mediated gut-to-brain transmission of α-syn.

2. Material and methods

2.1. Mice model

C57BL/6 mice carrying the NF-κB/c-Rel gene null mutation (c-rel$^{-/-}$ mice) were originally generated by inserting the neomycin cassette into the fifth exon of the NF-κB/c-Rel gene (Liou et al., 1999). Insertion of neomycin gene give the resistance to this antibiotic, which can be used to make cellular line selectable. The c-rel$^{-/-}$ and c-rel$^{+/+}$ wt mice were housed in the animal facility of the Department of Molecular and Translational Medicine of the University of Brescia. Animals were maintained in groups of 2–4/cage in individual ventilated cages under standard conditions (12 h/12 h light/dark cycles, humidity 55 %, room temperature 22–23 °C). The cages were enriched with nesting material and red mouse houses (Tecniplast). All mice had access to standard laboratory chows (complete feed for mice and rats 4RF21, Mucedola) and water *ad libitum*. All animal studies were approved by the Animal-welfare body of the University of Brescia (Organismo Preposto al Benessere degli Animali -OPBA-) and were in accordance with the Directive 2010/63/EU on the protection of animals used for scientific purposes. All the procedures performed accomplished the ethical standards of the University of Brescia. Only male mice were used in this study. A total of 37 animals were used in this study.

2.2. Tissue collection and colon length measurement

Different groups of wt and c-rel$^{-/-}$ male mice were sacrificed by cervical dislocation. The mouse colon was removed and its longitudinal length from ileocecal junction to the anal verge was measured (Parrella et al., 2025). Stool pellets were gently expelled from the colon, then the tissue was cut longitudinally, cleaned with ice-cold Phosphate-Buffered Saline (PBS) (Sigma-Aldrich), and divided into the proximal and distal portions. Half of the proximal colon was frozen and stored at −80 °C, half was processed for immunohistochemistry analysis.

2.3. Immunohistochemistry

Mice were anesthetized with chloral hydrate (400 mg/kg intraperitoneally, Sigma-Aldrich) and transcardially perfused with PBS (Sigma-Aldrich) and 4 % (*w/v*) ice-cold paraformaldehyde (Immunofix, Bio-Optica). Brains were collected, post-fixed and conserved in 30 % sucrose. Coronal slices (30 μm) were cut with a cryostat to obtain serial sections of the DMV (anterior-posterior −7.43 to −7.67 mm). Alpha-syn and choline acetyltransferase (ChAT) immunolabeling coupled with Hoechst staining was accomplished as follow: slices were incubated with

anti-α-synuclein (1:200, BD Biosciences) and anti-ChAT (1:50, Sigma-Aldrich) primary antibodies overnight at 4 °C, washed and then incubated with Cy3 (1:1000, Jackson ImmunoResearch) secondary antibody for 1 h at room temperature. After washing, slices were incubated with biotinylated anti-goat antibody (1:200, Dako) and subsequently incubated with Alexa Fluor™ 488 streptavidin (1:1000, Life-Technologies) to amplify ChAT immuonoreactivity (see Table 1 for antibody details). Cell nuclei were stained by incubating the sections with Hoechst (1:3000, Sigma-Aldrich) for 3 min. Lipofuscin autofluorescence was quenched by incubation with TrueBlack® (1:40, Biotium) for 30 s, and coverslips were then mounted by using Vectashield mounting medium (Vector Laboratories). Fluorescence labeling was acquired by using a confocal microscope (LSM 900, Carl Zeiss). Images (1024 × 1024 pixels) were then reconstructed using LSM Zen Blue Image Examiner (Carl Zeiss). Alpha-syn and ChAT images were acquired in red and green as false colors, respectively. Alpha-syn immunoreactivity was quantified on digitized images using the FIJI (NIH) software (Parrella et al., 2019). Briefly, α-syn-positive-area was normalized *vs* DMV area. For this study, 2–4 DMV sections from 3 to 6 mice were analyzed.

Samples of proximal colon from 2- and 10-month-old wt and c-rel$^{-/-}$ male mice were fixed with 4 % (*w/v*) ice-cold paraformaldehyde (Immunofix, Bio-Optica) for 2 h and then transferred to 30 % sucrose solution. Coronal slices (20 μm thick) were cut at the cryostat and mounted on Superfrost slides (Thermo Scientific). Alpha-syn and βIII-tubulin immunolabeling coupled with Hoechst staining was accomplished as follow: slices were incubated with anti-α-synuclein (1:500, BD Biosciences) and anti-βIII-tubulin (1:300, Sigma-Aldrich) primary antibodies overnight at 4 °C, washed and then incubated with Cy3 (1:3000, Jackson ImmunoResearch) and Alexa Fluor™ 488 (1:3000, Jackson ImmunoResearch) conjugated secondary antibodies for 1 h at room temperature (see Table 1 for antibody details). Cell nuclei were stained by incubating the sections with Hoechst (1:3000, Sigma-Aldrich) for 3 min. Alpha-syn phosphorylated form in serine 129 (pSer-α-syn) and βIII-tubulin immunolabeling coupled with Hoechst staining was performed as follow: slices were incubated with anti-pSer-α-syn (1:600, Abcam) and anti-βIII-tubulin (1:750, Promega) primary antibodies overnight at 4 °C, washed and then exposed to Cy3 (1:3000, Jackson ImmunoResearch) and Alexa Fluor™ 488 (1:1000, Jackson ImmunoResearch) conjugated secondary antibodies for 1 h at room temperature (see Table 1 for antibody details). Cell nuclei were stained by incubating the sections with Hoechst (1:3000, Sigma-Aldrich) for 3 min. In both α-syn and pSer-α-syn immunolabeling lipofuscin autofluorescence was quenched by incubation with TrueBlack® (1:40, Biotium) for 30 s, and coverslips were then mounted by using Vectashield mounting medium (Vector Laboratories). Fluorescence labeling was acquired by using a confocal microscope (LSM 510 META, Carl Zeiss). Images (1024 × 1024 pixels) were then reconstructed using LSM Zen Blue Image Examiner (Carl Zeiss). In the α-syn immunolabeling, α-syn and βIII-tubulin images were acquired in green and red as false colors, respectively. Alpha-syn and pSer-α-syn immunoreactivity was quantified on digitized images using the FIJI (NIH) software (Parrella et al., 2019). Briefly, α-syn and pSer-α-syn surface and the number of α-syn and pSer-α-syn inclusions were normalized *vs* the enteric ganglion area. For this study, 3–6 colon sections from 3 to 5 mice, with an average of 6 fields per section were analyzed.

CD45 immunolabeling was performed by incubating the slices with anti-CD45 primary antibody (1:100, Bio-Rad) overnight at 4 °C. Colon sections were then incubated with biotinylated secondary antibodies (1:200, Vector Laboratories) and visualized by avidin-biotin-horseradish peroxidase technique (ABC Elite; Vector Laboratories) using 3,3′-diaminobenzidine (ImmPACT™ DAB kit; Vector Laboratories) as chromogen (see Table 1 for antibody details). Microscopy images were acquired on Olympus BX43 microscope using Olympus DP74 digital camera with cellSens Entry system. Numbers of CD45-positive cells on histological stains were determined by manually counting positive cells in five nonoverlapping fields of proximal colon in 3–5 samples per genotype (Szabo et al., 2019; Mota et al., 2020).

TH immunolabeling was performed by incubating the slices with primary anti-TH antibody (1:300, Merck Millipore) overnight at 4 °C. Colon sections were then incubated with biotinylated secondary antibodies (1:800, Vector Laboratories) and visualized by avidin-biotin-horseradish peroxidase technique (ABC Elite; Vector Laboratories) using DAB (ImmPACT™ DAB kit; Vector Laboratories) as chromogen (see Table 1 for antibody details). Microscopy images were acquired on Olympus BX43 microscope using Olympus DP74 digital camera with cellSens Entry system. TH immunoreactivity was quantified on 3–8 colon sections (6 fields per section) from 4 to 6 mice using the FIJI (NIH) software.

Table 1
List of primary antibodies used for immunohistochemistry, flow cytometry and WB analysis.

Primary antibodies	Working concentration	Source	Catalogue number
anti-α-synuclein	1:200-1:500 (IF) 1:250 (WB)	BD Biosciences	610786
anti-βIII-tubulin	1:300-1:750 (IF)	Sigma-Aldrich	T2200
anti-pSer-α-synuclein	1:600 (IF)	Abcam	59264
anti-ChAT	1:50 (IF)	Sigma-Aldrich	AB144P
anti-CD45 antibody	1:100 (IHC)	Bio-Rad	MCA1031G
anti-TH antibody	1:300 (IHC) 1:2000 (WB)	Merck Millipore	AB152
anti-CD45 BV605	1:100 (FACS)	Biolegend	#103155
anti-CD11b VioBright FITC	1:200 (FACS)	Miltenyi Biotech	#130-113-243
anti-F4/80 PercPVio700	1:100 (FACS)	Miltenyi Biotech	#130-118-466
anti-CD3 PE	1:100 (FACS)	Miltenyi Biotech	#130-109-837
anti-Ly6G APC	1:100 (FACS)	Miltenyi Biotech	#130-120-734
anti-occludin	1:250 (WB)	Invitrogen	#71-1500
anti- zonula occludens (ZO-1)	1:200 (WB)	Invitrogen	#33-9100
anti-GAPDH	1:2000 (WB)	Merck Millipore	#MAB374

2.4. Preparation of intestinal protein samples

Lysate of mouse proximal colon was prepared by homogenization in modified ice-cold RIPA buffer (150 mM sodium chloride; 50 mM Tris, pH 7.6; 5 mM ethylenediaminetetraacetic acid and 1 % Triton X-100 including protease and phosphatase inhibitors) and then sonication for 1 min on ice. After 30 min, samples were sonicated for the second time and then tissue and cell debris was removed by centrifugation at 4 °C for 20 min at 12,000*g*. Protein concentration was determined with Bio-Rad protein assay according to the manufacturer's instruction.

2.5. NADPH oxidase activity

NADPH oxidase (Nicotinamide adenine dinucleotide phosphate oxidase) activity was measured due to its capability to convert molecular oxygen to anion superoxide through the oxidation of NADPH to NADP plus H+. In a 96-well microplate, 35 μl of PBS (pH 7.4) and 5 μl of mice colon protein extract were mixed. Then 5 μl of 0,1 mM NADPH was added to the mixture. The reaction was monitored spectrophotometrically by following the reduction in NADPH absorbance at 340 nm through its consumption by NADPH oxidase. The activity of NADPH oxidase was calculated as the concentration of NADP reduced by NADPH oxidase per minute and normalized to the microgram of protein for each sample (μM NADP/μg protein/min) (Pucci et al., 2021).

2.6. Tissue 3-nitrotyrosine level

Free 3-nitrotyrosine (3-NT) as a marker of peroxynitrite generation and oxidative stress was measured by enzyme-linked immunosorbent assay (ELISA) as reported by Poles, M.Z et al. (Poles et al., 2018) with some modifications. Briefly, 15 µg of proximal colon protein extracts were diluted in PBS 1 × pH 7.4 and coated on the ELISA microplate overnight at 4 °C. Bovine serum albumin (BSA)-3-NT Standard (Abcam, Netherlands) was also coated at different concentrations ranging from 16 to 0.5 ng/ml to include a calibration standard curve. The next day plates were saturated with 100 µl of blocking solution (PBS 1 × pH 7.4; 0.1 % TWEEN 20; 3 % BSA; 5 % Normal Goat Serum) for each well and incubated for 1 h at room temperature, followed by 2 h incubation at 37 °C with anti-3-NT antibody (Sigma-Aldrich) diluted 1:400. After washing with PBST (PBS 1 × pH 7.4–0.5 % TWEEN 20), 0.1 mg/ml secondary anti-mouse antibody conjugated with peroxidase (Dako Agilent, Santa Clara, CA, USA) was incubated in each well for 1 h at room temperature. Finally, 100 µl of 3,3,5,5-tetramethylbenzidine substrate was added and the reaction was stopped with 100 µl of sulfuric acid 2 M. Optical density was measured using a microplate reader with a wavelength of 450 nm. Nitrotyrosine content was normalized to the protein content and expressed as 3-NT µg/µg protein tissue extract.

2.7. Flow cytometry

Lamina propria immune cells were isolated using the Mouse Lamina Propria Dissociation Kit (Miltenyi Biotech). Briefly, colon was harvested and cleaned of fat residue and feces. To obtain lamina propria cells (LPCs), the colon was cut longitudinally and fragmented into pieces. After multiple incubations at 37° with Pre-digestion and digestion medium prepared as manufacture's instruction, the lamina propria cells were mechanically isolated using a GentleMACS dissociator. The ensuing single-cell suspension was filtered by means of a 70-µm cell strainer and prepared for cytofluorimetric analysis. After Fc blocking, single-cell suspensions were stained with the following antibodies: CD45 BV605 (clone 30-F11), CD11b VioBright FITC (clone REA592), F4/80 PERCPVio770 (clone REA126), CD3 PE (clone REA641), Ly6G APC (clone REA526) (see Table 1 for details). Subsequently, doublet exclusion and gating on live CD45+ cells was performed. Cell viability was determined by LIVE/Dead-405 nm (L34959) staining according to the manufacturer's instructions (Invitrogen); negative cells were considered viable. The following subpopulations of CD45+ were identified: CD11b+Ly6G+ (neutrophils), CD11b+F4/80+ (macrophages), CD3+CD4+ and CD3+C8+ (T cells). Cells were analyzed on a MACSQuant16 (Miltenyi) and analyzed with FlowJo software (RRID: SCR_008520, Treestar).

2.8. Real-time quantitative reverse transcription-polymerase chain reaction (qRT-PCR)

Intestinal tissues derived from mice at 2 and 10 months of age were processed for mRNA analysis. Total intestinal RNA was isolated using TRI reagent (Sigma-Aldrich). Two µg of total RNA were reverse transcribed using M-MLV reverse transcriptase (Promega). qRT-PCR was conducted to analyze the gene expression of a pleiotropic pro-inflammatory cytokine such as interleukin-6 (IL-6) and interleukin-17A (IL-17A), a key intestinal pro-inflammatory marker. The murine specific primers were shown in Table 2.

Amplification and detection were performed with the ViiA7 Real Time PCR Detection System (Applied Biosystems). The reaction mix contained 6 µl of SYBR Green Master Mix (Bio-Rad), 6 pmol of each forward and reverse primer, and 2 µl of diluted cDNA. The samples were run in duplicate, and the PCR program was initiated by 10 min at 95 °C before 40 cycles, each one of 1 s at 95 °C and 30 s at 64 °C. The gene expression levels were normalized to β-Actin expression and the data were presented as the fold change in target gene expression. Relative quantification was performed using the comparative Ct method (Pucci et al., 2022).

Table 2
List of primers used for qRT-PCR.

Genes	Primer sequences
Interleukin 6 (IL-6)	for: 5′-CCTACCCCAATTTCCAATGCT-3′ rev: 5′-TATTTTCTGACCACAGTGAGGAAT-3′
Interleukin 17-A (IL-17A)	for: 5′-TCCAGAAGGCCCTCAGACTA-3′ rev: 5′-TTCATTGCGGTGGAGAGTC-3′
Actin (β-actin)	for: 5′-AGCCATGTACGTAGCCATCC-3′ rev: 5′-CTCTCAGCTGTGGTGGTGAA-3′

2.9. ELISA

IL-6 (DY206–05; DuoSet ELISA human IL-6; R&D Systems) and TNF-α (DY410; DuoSet ELISA human TNF-α; R&D Systems) were determined by commercially available ELISAs (R&D Systems), following manufacturer's instructions. The samples were run in duplicate. All absorbance readings were measured at 450 nm using a Emax Plus microplate reader (Molecular Devices). The concentrations of the cytokines (pg/ml) were then normalized to intestinal total protein contents and expressed as pg/µg protein tissue extract. TNF-α and IL-6 were assessed in 5 animals per group.

2.10. Multispectral Optoacoustic Tomography (MSOT)

Intestinal inflammation was evaluated as colonic increase of oxygenated hemoglobin (HbO_2) levels using MSOT imaging (Bhutiani et al., 2017). MSOT is an imaging technology which consist in illuminating tissue with light derived from transient energy, this energy is absorbed by tissue and result in a thermoelastic expansion. This give rise to ultrasound waves that are detected and then form an image. Mice were anesthetized with isoflurane (1.8 % at 0.8 l/min), and their abdominal area gently shaved using an electrical razor, followed by the application of depilatory cream (Veet) which was removed with a moist gauze. The day after, the animals were anesthetized with isofluorane (1.8 % at 0.8 l/min for mouse preparation; 1.8 % - 1.0 % to keep respiration rate at 60–70 breaths per minute during imaging) and their shaved skin covered with ultrasound gel (Comedical) for improved ultrasound coupling. Then mice were wrapped in a thin polyethylene membrane, placed supine and imaged from the thorax to inferior pelvis and translated using a linear stage to enable imaging of multiple transverse slices with the MSOT inVision-128 small animal imaging scanner (iThera Medical GmbH). Acquisition and post-processing were carried out in viewMSOT 4.0.3.2 software (iThera Medical). Imaging was performed with a step size of 0.5 mm illuminating the mouse with ten arms of a fiber bundle to provide even illumination of a ring-shaped light strip of approximately 8 mm width at wavelengths of 700, 730, 760, 800, 850, and 875 nm with 25 averages per wavelength, at a repetition rate of 10 Hz with a wavelength tuning speed of 10 ms and a peak pulse energy of 100 mJ at 730 nm. For ultrasound detection, a 128-element ultrasound transducer with a center frequency of 5 MHz (60 % bandwidth), organized in a concave array of 270-degree angular coverage and a radius of curvature of 4 cm, was used. The acquired images were reconstructed with a back projection algorithm using the BP 4.0 *in vivo* preset to create cross-sectional images. Reconstruction field of view was set to 25 mm (75 µm resolution), and reconstructed images were then spectrally unmixed using the linear regression algorithm for oxygenated- (HbO_2) and deoxygenated hemoglobin (Hb). MSOT values for colon HbO_2 were determined by region of interest (ROI) analysis. Briefly, colon was identified through the comparison with a mouse atlas (Micheau and Hoa, 2018). Four colon ROI of similar surface were drawn every 4 mm and then interpolated to obtain the volume of interest (VOI). The mean HbO_2 signal intensity within the VOI

was calculated for 4–5 animals per group.

2.11. Colon motility

Colon motility was assessed in 2- and 10-month-old mice using the one-hour stool collection assay (Parrella et al., 2019; Parrella et al., 2025). Briefly, experiments were conducted in a dedicated quiet room during the light phase, consistently between 10:00 and 12:00 AM. Mice were individually transferred from their home cages to clean, empty plastic cages [36 × 15.5 × 13.5 cm] without access to food or water for a duration of one hour. Stool pellets were collected immediately following expulsion and deposited into pre-weighed, sealed 1.5 ml microtubes (Biosigma). The number of expelled pellets was recorded, and stool frequency was expressed as pellets per hour, normalized to a 30 g body weight. Tubes were weighed to determine the wet weight of the stool. Pellets were subsequently dried overnight at 65 °C and reweighed to obtain dry weight. Stool water content (%) was calculated as the difference between wet and dry weight, relative to the wet weight.

2.12. Western blot analysis

The levels of TH and tight junction proteins content in proximal colon extracts were evaluated by western blot technique. Briefly, total protein extracts were resolved by 10 % and 4 %–12 % SDS PAGE gel and transferred to a nitrocellulose membrane (Amersham). Membranes were then incubated with anti-TH (1:2000, Merck Millipore), anti-occludin (1:250, Invitrogen), anti-zonula occludens (ZO-1, 1:200, Invitrogen) or anti-GAPDH (1:2000, Merck Millipore) primary antibody and secondary antibodies coupled to alkaline phosphatase (AP) (1:2000, Promega) (see Table 1 for antibody details). Immunopositive bands were visualized by AP chemiluminescent substrate (Novex®, ThermoFisher). Gel analysis was performed using the Gel Pro.3 analysis software (MediaCybernetics).

2.13. Statistical analysis

Statistical analysis was performed with the GraphPad Prism software. Data were expressed as mean ± standard deviation (SD). Statistical significance was accepted at the 95 % confidence level ($p < 0.05$). Normal distribution of data was assessed with Shapiro-Wilk test. Comparisons between two groups were performed using the parametric two-tailed unpaired Student's *t*-test, or the nonparametric Mann-Whitney test. Comparisons among more than two groups were performed using the parametric multiple *t*-test followed by Sidak-Bonferroni multiple

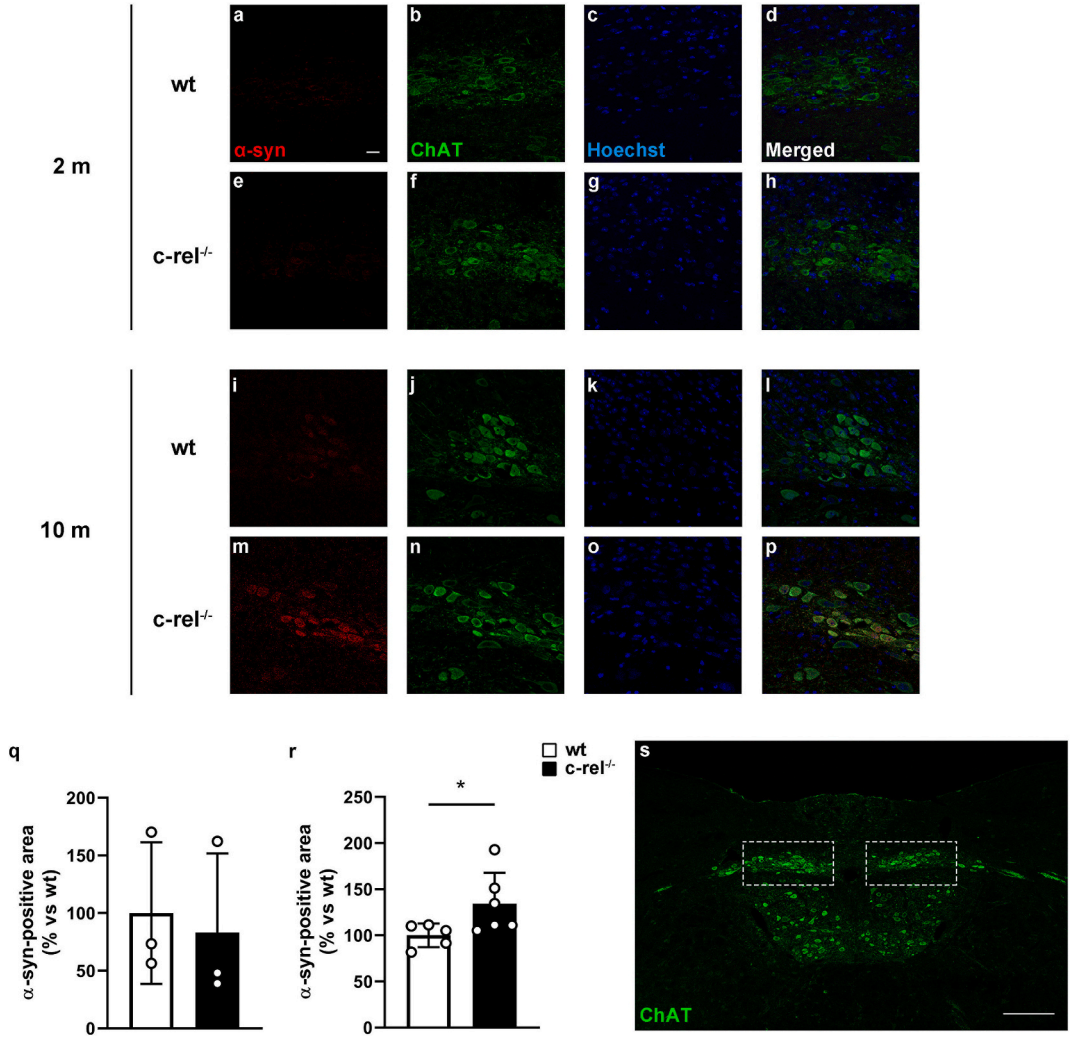

Fig. 1. c-rel$^{-/-}$ mice display progressive α-syn accumulation in the DMV. Representative photomicrographs displaying α-syn (red), ChAT (green) and Hoechst (blue) immunofluorescence labeling in sections of DMV from 2-month-old wt (**a-d**), 2-month-old c-rel$^{-/-}$ mice (**e-h**), 10-month-old wt (**i-l**) and 10-month-old c-rel$^{-/-}$ mice (**m-p**). Measurement of the α-syn-positive surface (**q** and **r**) proved a significant increase of α-syn immunoreactivity in 10-month-old c-rel$^{-/-}$ mice in comparison to wt (**r**), but not in 2-month-old c-rel$^{-/-}$ (**q**). $n = 3$ animals per group in **q**. $n = 5$–6 animals per group in **r**. Results are expressed as mean ± SD. *$p < 0.05$, $d = 1.022$, 95 % CI [−1.911, 70.520], *t*-test in **f**. ChAT-stained section showing the DMV area (**s**). Scale bar = 20 μm in **a**, scale bar = 200 μm in **s**.

comparison test, or the non-parametric Kruskal–Wallis test followed by Dunn's multiple comparison test. Effect sizes are presented as partial eta squared (η_p^2) for ANOVAs, Cohen's d (*d*) for *t*-tests and eta squared (η^2) for Mann-Whitney and Kruskal-Wallis tests. Where applicable, 95 % confidence intervals (95 % CI) are reported in brackets using the format 95 % CI [lower bound, upper bound].

3. Results

3.1. c-rel$^{-/-}$ mice show progressive α-syn accumulation in the DMV

We previously reported that c-rel$^{-/-}$ mice display a prodromal syndrome and a Braak-like accumulation of α-syn, mimicking sporadic PD (Parrella et al., 2019).

To investigate a potential gut-to-brain transmission of α-syn, we assessed its accumulation in the DMV of c-rel$^{-/-}$ and wt male mice at 2 and 10 months of age by performing double immunolabeling for α-syn and ChAT (Fig. 1). In line with our previous findings, no significant difference in α-syn-positive area was observed in the DMV of 2-month-old animals, whereas a significant increase in c-rel$^{-/-}$ mice was detected at 10 months when compared to wt littermates.

3.2. α-syn pathology progressively affects the myenteric plexus of proximal colon in c-rel$^{-/-}$ mice

Previous studies showed a marked immunoreactivity for both α-syn and pSer-α-syn in the ENS of PD patients respect to control subjects.

To evaluate the progression of α-syn pathology in ENS of c-rel$^{-/-}$ male mice, we performed double immunolabeling for α-syn and βIII-tubulin, a pan-neuronal marker, in the proximal colon of c-rel-$^{-/-}$ and wt male mice of 2- and 10-months of age (Fig. 2). We observed α-syn accumulation in the colonic myenteric ganglia of 2-month-old c-rel$^{-/-}$ mice, that increased in 10-month-old c-rel$^{-/-}$ mice, as shown in Fig. 2**a-h**. Quantification of immunofluorescence signals confirmed a significant increase

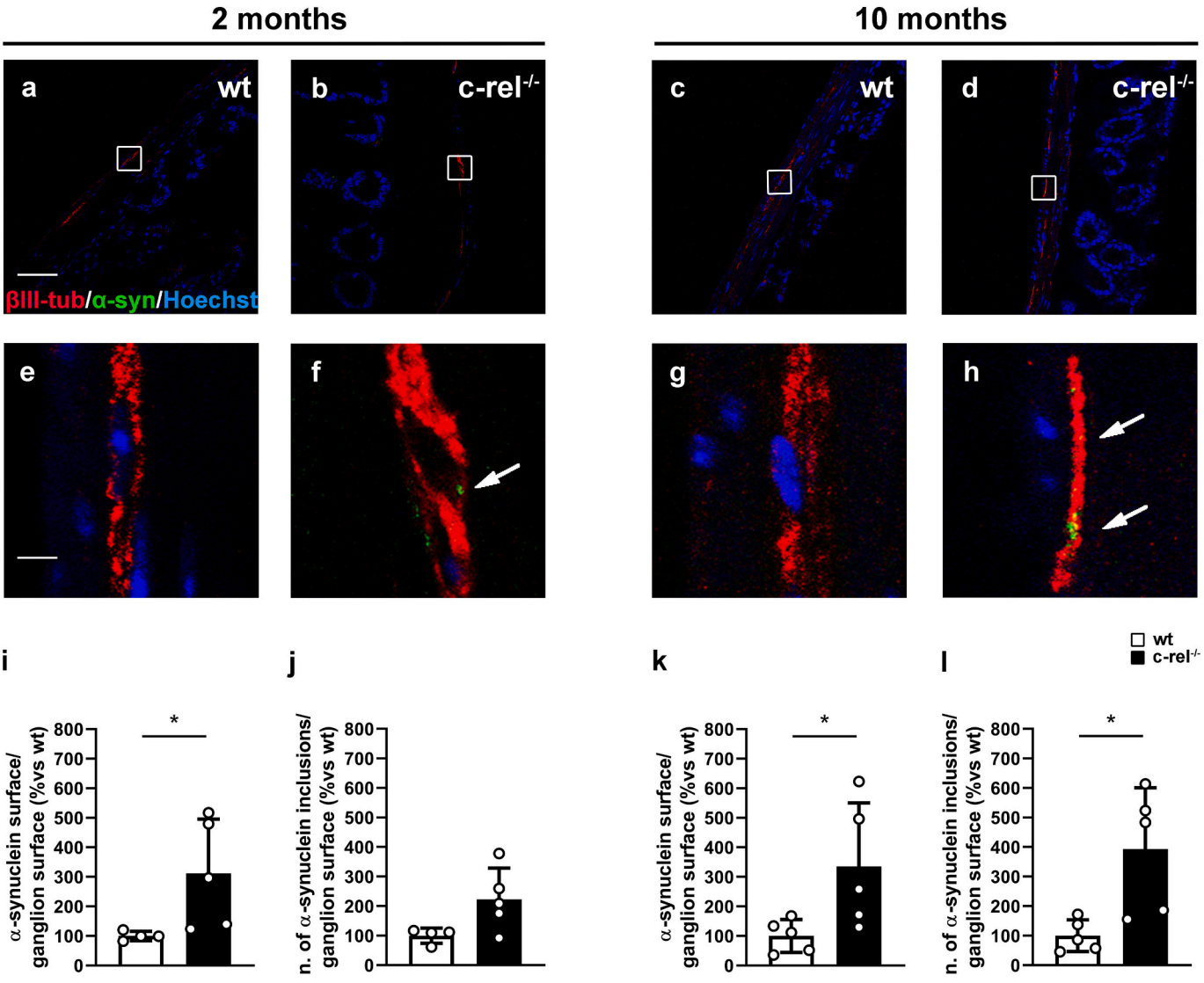

Fig. 2. c-rel$^{-/-}$ mice display early and progressive α-syn accumulation in the myenteric plexus of proximal colon. Representative photomicrographs displaying α-syn/βIII-tubulin/Hoechst immunofluorescence labeling in sections of proximal colon from 2-month-old wt (**a**), 2-month-old c-rel$^{-/-}$ mice (**b**), 10-month-old wt (**c**) and 10-month-old c-rel$^{-/-}$ mice (**d**). High magnifications of the areas in the squares in panels **a**, **b**, **c** and **d** are displayed in **e**, **f**, **g** and **h**, respectively. Please note the presence of α-syn-positive inclusions in the ganglia of c-rel$^{-/-}$ mice (arrows in panel **f** and **h**). Measurement of the α-syn-positive surface (**i** and **k**), and the number of α-syn inclusions (**j** and **l**) normalized by the ganglion area proved a significant and progressive increase of α-syn immunoreactivity in c-rel$^{-/-}$ mice in comparison to wt animals. $n = 4$–5 animals per group. Results are expressed as mean ± SD. $^*p < 0.05$, $\eta^2 = 0.667$, 95 % CI [19.59, 418.3], Mann-Whitney test in **i**. $^*p < 0.05$, $d = 1.100$, 95 % CI [7.732, 464.100], *t*-test in **k**. $^*p < 0.05$, $d = 1.407$, 95 % CI [71.160, 514.400], *t*-test in **l**. Scale bars: in **a**, **b**, **c** and **d** = 20 μm; in **e**, **f**, **g** and **h** = 5 μm.

in the α-syn surface/ganglion surface ratio at 2 and 10 months (Fig. 2**i,** 2**k**), and in the total number of protein inclusions/ganglion surface ratios in the older mice (Fig. 2**l**).

We then investigated the presence of the phosphorylated form of α-syn by double immunolabeling for pSer-α-syn and βIII-tubulin in intestinal samples from 2- and 10-month-old animals (Fig. 3). The accumulation of pSer-α-syn was already evident in the colonic myenteric ganglia of 2-month-old c-rel$^{-/-}$ mice and increased in 10-month-old animals (Fig. 3**a-h**). This was confirmed by the increase in the pSer-α-syn surface/ganglion surface ratio quantified at 2 and 10 months and the number of protein inclusions/ganglion surface ratios at 10 months (Fig. 3**i-l**).

Next, we evaluated the pSer-α-syn/α-syn ratio to investigate the relative increase in α-syn phosphorylation between 2- and 10-month-old c-rel$^{-/-}$ mice. We did not observe any significant difference in the pSer-α-syn/α-syn ratio in either 2- or 10-month-old c-rel$^{-/-}$ mice compared with their wt littermates, suggesting that the increase in phosphorylation occurs along with endogenous accumulation of α-syn. (Supplementary Fig. 1).

3.3. Progressive loss of TH in the submucosal and myenteric plexuses of the proximal colon in c-rel$^{-/-}$ mice

Next, we investigated the relative amount of TH-positive neurons in the submucosal and myenteric plexuses of the proximal colon in 2- and 10-month-old wt and c-rel$^{-/-}$ mice (Fig. 4). Our results showed a progressive reduction of TH immunoreactivity in c-rel$^{-/-}$ mice, becoming significant at 10 months (Fig. 4f). Western blot analysis confirmed decreased levels of TH at 10 months in c-rel$^{-/-}$ mice (Fig. 4g-j) These findings are aligned with results from other experimental models of PD, although inconsistent evidence have been reported in human samples over the years (Costa et al., 2023).

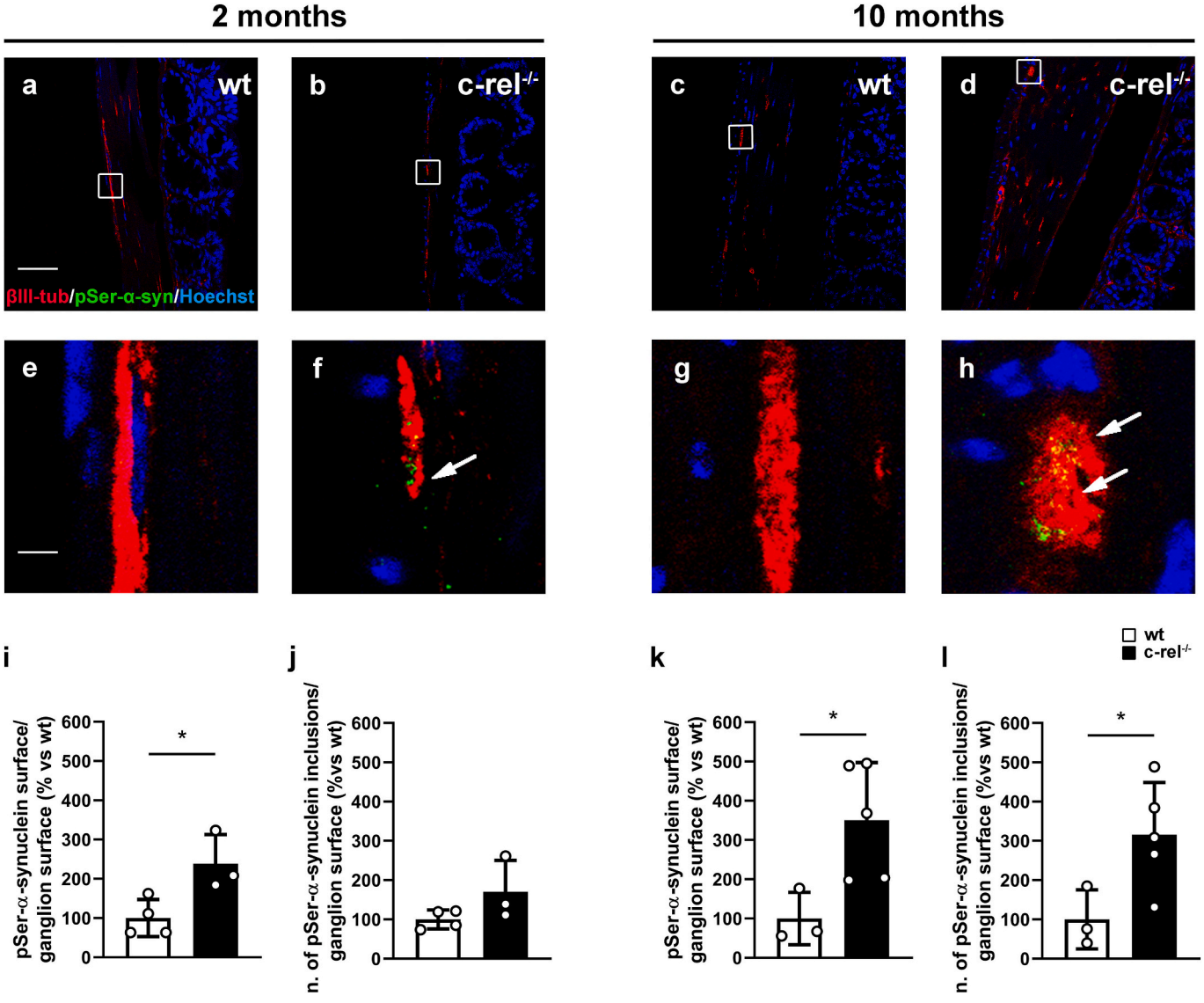

Fig. 3. c-rel$^{-/-}$ mice display early and progressive pSer-α-syn accumulation in the myenteric plexus of proximal colon. Representative photomicrographs displaying pSer-α-syn/βIII-tubulin/Hoechst immunofluorescence labeling in sections of proximal colon from 2-month-old wt (**a**), 2-month-old c-rel$^{-/-}$ mice (**b**), 10-month-old wt (**c**) and 10-month-old c-rel$^{-/-}$- mice (**d**). High magnification of the areas in the squares in panels **a**, **b**, **c** and **d** are also provided (in **e**, **f**, **g** and **h**, respectively). Please note the presence of pSer-α-syn-positive inclusions in the ganglia of c-rel$^{-/-}$ mice (arrows in panel **f** and **h**). Quantification of the pSer-α-syn-positive surface normalized by the ganglion area (**i** and **k**), and the number of pSer-α-syn inclusions (**j** and **l**) confirmed a significant and progressive increase of pSer-α-syn immunoreactivity in c-rel$^{-/-}$ mice when compared to wt littermates. $n = 3$–5 animals per group. Results are expressed as mean ± SD. *$p < 0.05$, $d = 1.864$, 95 % CI [21.490, 255.500], *t*-test in i. *$p < 0.05$, $d = 1.717$, 95 % CI [26.88, 475.0], *t*-test in **k**. *$p < 0.05$, $d = 1.881$, 95 % CI [6.075, 425.200], *t*-test in **l**. Scale bars: in **a**, **b**, **c** and **d** = 20 μm; in **e**, **f**, **g** and **h** = 5 μm.

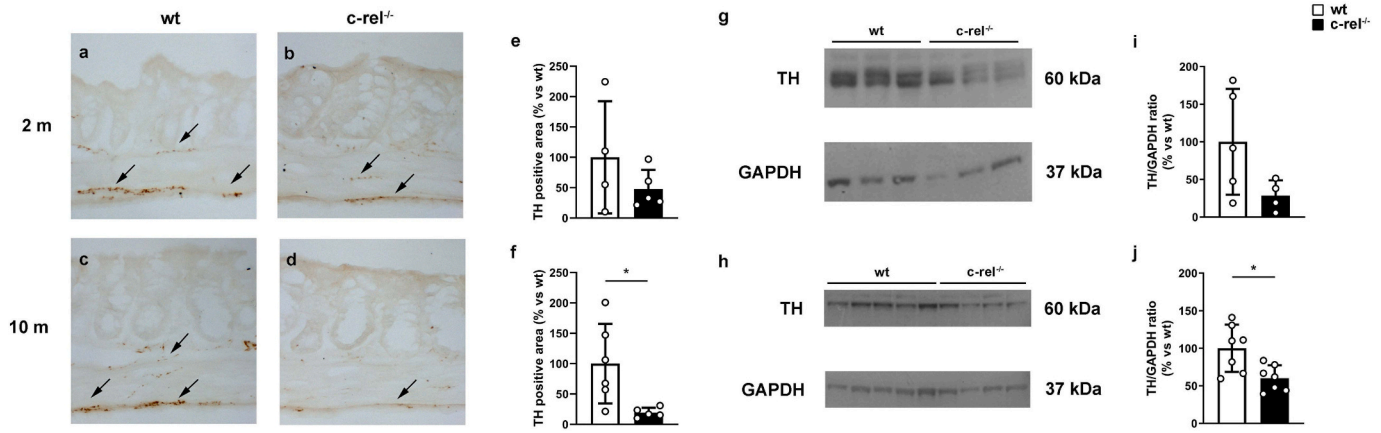

Fig. 4. TH loss in proximal colon of c-rel$^{-/-}$ mice. Representative images of anti-TH immunostaining (arrowheads) of proximal colon from 2-month-old wt (**a**), 2-month-old c-rel$^{-/-}$ (**b**), 10-month-old wt (**c**) and 10-month-old c-rel$^{-/-}$ male mice (**d**). Densitometric analysis revealed a significant reduction of TH-positive area in the proximal colon of 10-month-old c-rel$^{-/-}$ mice. Results are expressed as mean ± SD. n = 4–5 animals per group in **e**. n = 5–6 animals per group, *$p < 0.05$, $d = -10.004$, 95 % CI [−148.000, −13.430], t-test in **f**. (**g-j**) Evaluation of the expression of TH was performed in total protein extracts from proximal colon of 2- and 10-month-old wt and c-rel$^{-/-}$ male mice. Quantitative analysis of TH revealed a significant decrease in c-rel$^{-/-}$ male mice at 10 months of age. n = 4–5 animals per group in **i**. n = 7 animals per group in **j**. Results are presented as mean ± SD. *$p < 0.05$, $d = -2.319$, 95 % CI [−69.380, −10.380], t-test in **j**.

3.4. *Progressive oxidative stress is evident in proximal colon of c-rel$^{-/-}$ mice*

The enzymatic activity of NADPH oxidase was performed to investigate whether α-syn accumulation could be associated with oxidative stress. NADPH oxidases are a family of enzymes widely expressed in the gut, that produce reactive oxygen species (ROS) in many cells and tissues (Aviello and Knaus, 2017) (Bedard and Krause, 2007). In c-rel$^{-/-}$ mice, NADPH oxidase activity was already increased at 2-month-old mice, but became statistically higher in 10-months-old mice when compared to wt mice (Fig. 5**a**).

We also checked the colonic levels of 3-NT-modified proteins, a biomarker related to nitrosative stress. 3-NT formation is caused by the nitration of protein-bound and free tyrosine residues by peroxynitrite molecules (Beckman, 1996) and it has been already found relevant in the intestine (Poles et al., 2018). Interestingly, c-rel$^{-/-}$ mice showed a marked increase in the levels of 3-NT-modified proteins at 10 months of age when compared with age-matched wt mice, while a positive trend to significance could already be observed at 2 months of age (Fig. 5**b**).

3.5. *c-rel$^{-/-}$ mice show progressive low-grade intestinal inflammation*

To test whether c-rel$^{-/-}$ mice exhibited intestinal inflammation in the proximal colon, we investigated several parameters, including immune cells infiltration, cytokines expression and colonic macroscopic changes.

At first, we examined the stromal infiltration of immune cells in the proximal colon of 2- and 10-month-old mice by performing the immunostaining for CD45, a general marker for innate and adaptative immune cells (Fig. 6). We observed a significant increase of CD45-positive infiltrating cells in the colon of 10-month-old c-rel$^{-/-}$ mice respect to wt mice (Fig. 6**d,** 6**f**).

The evaluation of the immune cell populations in the lamina propria from proximal colon was performed by flow cytometry. This analysis confirmed an increasing trend in the number of CD45 positive cells of 10-month-old c-rel$^{-/-}$ mice. (p = 0.06, Fig. 7a-c). Analysis of CD45-positive cell subpopulation showed levels of colonic neutrophils significantly higher in c-rel$^{-/-}$ mice (Fig. 7d-f), but no difference in the number of macrophages, T lymphocytes, or specific CD4+ and CD8+ lymphocytes, when compared with wt mice (Fig. 7g-j).

Next, we examined the mRNA expression of specific interleukins detected in intestinal tract such as *IL-17A*, an important marker in the pathogenesis of the inflamed gut, and *IL-6,* which is a well-known pro-inflammatory marker involved in the pathogenesis and exacerbation of gut inflammation (Fujino et al., 2003; Matsunaga et al., 2009). While no significant differences in the *IL-17A* gene expression were detectable, we observed augmented levels of IL-6 transcripts in 2-months old mice and significantly higher level at 10 months of age (Fig. 8**a,** 8**b**). Protein levels of cytokines (IL-6 and TNF-α) were also measured by ELISA analysis. ELISA showed only a trend for the increase of IL-6 and no increase of TNF-α in c-rel$^{-/-}$ mice (Fig. 8**c,** 8**d**).

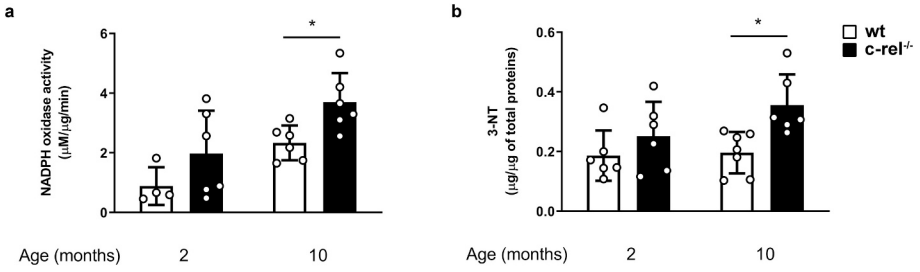

Fig. 5. c-rel$^{-/-}$ mice exhibit progressive pro-oxidant status of proximal colon. Colonic oxidative stress was investigated in 2- and 10-month-old wt and c-rel$^{-/-}$ male mice by measuring NADPH oxidase activity (**a**) and 3-NT proteins levels (**b**). (**a**) NADPH oxidase activity measured in proximal colon protein extracts was significantly higher in 10-month-old c-rel$^{-/-}$ mice. n = 4–6 animals per group. Results are expressed as mean ± SD. *$p < 0.05$, $d = 1.396$, 95 % CI [0.328, 2.395], multiple t-test adjusted with Sidak-Bonferroni method. (**b**) Similarly, 3-NT protein levels measured by ELISA assay were significantly increased in the proximal colon derived from 10-month-old c-rel$^{-/-}$ mice. n = 6–7 animals per group. Results are expressed as mean ± SD. *$p < 0.05$, $\eta^2 = 0.28$, Kruskal-Wallis test followed by Dunn's multiple comparison test.

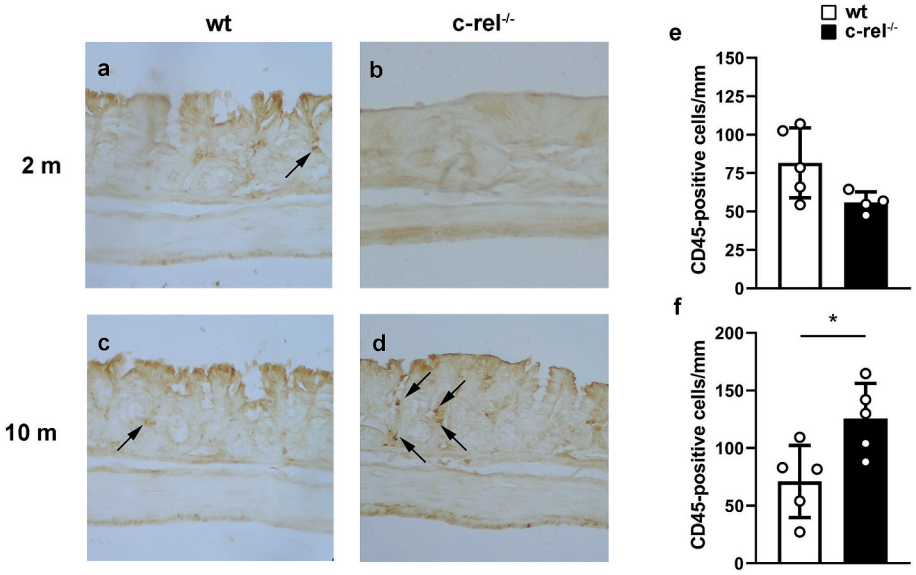

Fig. 6. c-rel$^{-/-}$ mice show immune cells infiltration in the proximal colon. Representative images of anti-CD45 immunostaining (arrowheads) of proximal colon from 2-month-old wt (**a**), 2-month-old c-rel$^{-/-}$ (**b**), 10-month-old wt (**c**) and 10-month-old c-rel$^{-/-}$ male mice (**d**). (**e-f**) Quantification of CD45-positive cells indicated an increased infiltration of immune cells in the intestine of 10-month-old c-rel$^{-/-}$ mice, which is not present in 2-month-old mice. $n = 4$–5 samples per group. Results are expressed as mean ± SD. *$p < 0.05$, $\eta^2 = 0.481$, 95 % CI [5.000, 110.600], Mann-Whitney test.

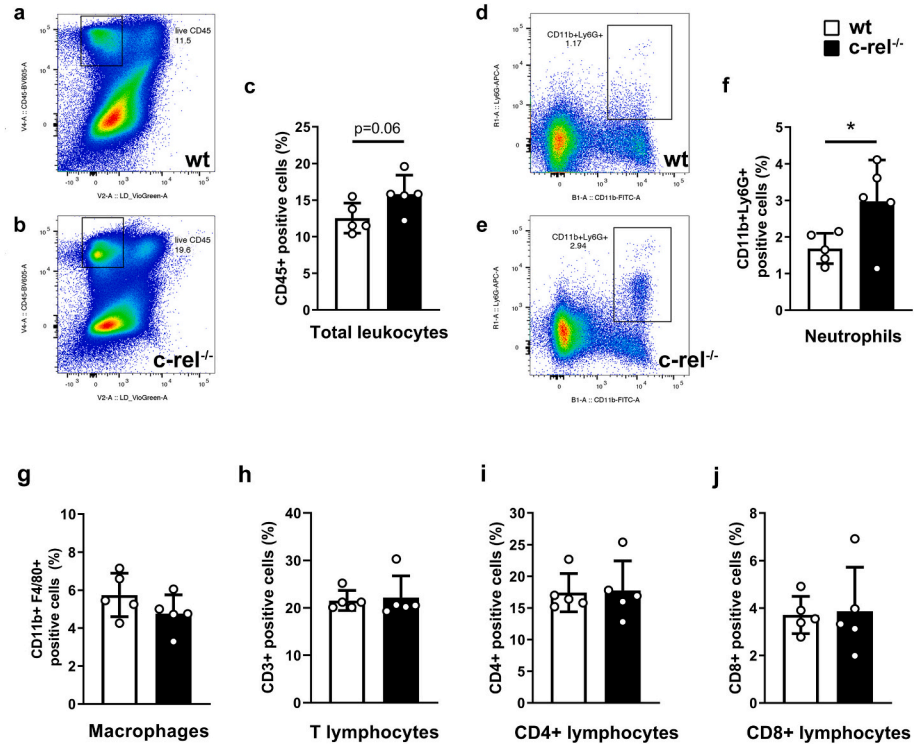

Fig. 7. Lamina propria immune cells population obtained from proximal colon was altered in 10-month-old c-rel$^{-/-}$ mice. Graphical representations of flow cytometry analysis of CD45-positive cells from wt (**a**) and c-rel$^{-/-}$ mice (**b**). Quantification of CD45-positive cells indicated an increased infiltration of immune cells in the intestine of 10-month-old c-rel$^{-/-}$ mice (**c**). Graphical representations of flow cytometry analysis of neutrophils (CD11b+Ly6G+) cells from wt (**d**) and c-rel$^{-/-}$ mice (**e**). Quantification of CD11b+Ly6G+ cells indicated an increased infiltration of neutrophils in the intestine of 10-month-old c-rel$^{-/-}$ mice (**f**). Percentages of macrophages (**g**), T lymphocytes (**h**), CD4+ lymphocytes (**i**) and CD8+ lymphocytes (**j**) are represented. $n = 5$ animals per group. Results are expressed as mean ± SD. *$p < 0.05$, $d = 1.245$, 95 % CI [−0.181, 6.701], *t*-test in **f**.

We also estimated gut morphological changes associated with chronic low-grade intestinal inflammation, including shortening of the colon in 4–6 and 10–13-month-old animals (Xu et al., 2008; Jin et al., 2017). The measurement of colon length at sacrifice revealed no change in younger mice but a reduction in c-rel$^{-/-}$ mice of 10–13 months (Fig. 9**a**). To confirm the increased gut inflammation, we performed MSOT imaging in live animals. This technique showed increased levels of oxyhemoglobin (HbO_2) in 12–13-month-old c-rel$^{-/-}$ mice (Fig. 9d), a sign reported to correlate with colitis severity in a mouse model of inflammatory bowel disease (Hilton et al., 2014).

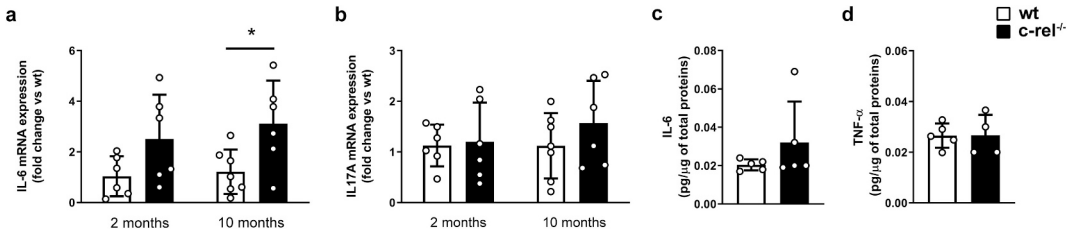

Fig. 8. c-rel$^{-/-}$ mice exhibit alteration in IL-6 expression. mRNA levels of IL-6 (**a**) and IL17A (**b**) and were measured in the proximal colon of 2- and 10-month-old wt and c-rel$^{-/-}$ mice. No differences in the levels of IL17A were found between wt and c-rel$^{-/-}$ male mice neither at 2 nor at 10 months of age (**b**). Differently, c-rel$^{-/-}$ mice displayed an increase of IL-6 mRNA, which was statistically significant at 10 months (**a**). IL-6 and TNF-α cytokines protein levels were evaluated in 10-month-old wt and c-rel$^{-/-}$ male mice using ELISA (**c,d**). No differences in the levels of these markers were found between wt and c-rel$^{-/-}$. $n = 6$–7 animals per group in **a** and **b**. $n = 4$–5 animals per group in **c** and **d.** Results are expressed as mean ± SD. *$p < 0.05$, 95 % CI [−3.686, −0.115], multiple *t*-test adjusted with Sidak-Bonferroni method in **a**.

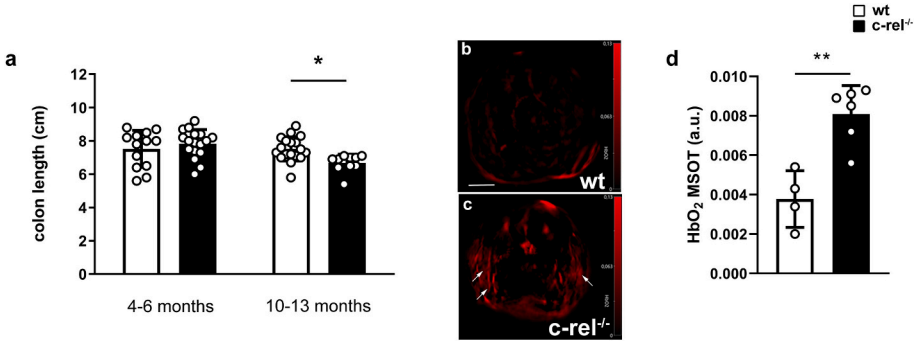

Fig. 9. c-rel$^{-/-}$ mice showed gut morphological changes associated with intestinal inflammation. Colonic inflammation was evaluated macroscopically by measuring the longitudinal length of the colon (**a**) from the caecum to the anal verge. c-rel$^{-/-}$ mice displayed colon shortening at 10–13 months, suggesting a chronic inflammatory state of the intestine. $n = 8$–15 samples per group. *$p < 0.05$, $\eta_p^2 = 0.1063$, 95 % CI [0.084, 1.600], two-way ANOVA followed by Sidak's multiple comparison test. Representative MSOT imaging of wt (**b**) and c-rel$^{-/-}$ (**c**) mice. Arrows indicate concentrated areas of HbO_2 corresponding to colon inflammation (**c**). Quantification of mean MSOT signal intensity for HbO_2 indicated higher HbO_2 levels in the colon of c-rel$^{-/-}$ mice (**d**). HbO_2 MSOT results were normalized for VOI values. $n = 4$–6 animals per group. Results are expressed as mean ± SD. **$p < 0.01$, $d = 3.014$, 95 % CI [0.002, 0.006], *t*-test.

We previously demonstrated that c-rel$^{-/-}$ male mice, aged 2 to 20 months, exhibited reduced stool frequency and stool water content in the one-hour stool collection assay, indicative of early-onset constipation (Parrella et al., 2019). To investigate whether reduced colon motility was associated with underlying colon pathology, cohorts of 2- and 10-month-old wt and c-rel$^{-/-}$ male mice were first tested with the one-hour stool collection assay before proceeding with gut analyses (Fig. 10**a,** 10**b**). The results showing a decrease in stool frequency and stool water content in c-rel$^{-/-}$ mice at both 2 and 10 months confirmed the reduced colon motility previously observed in this model (Parrella et al., 2019).

Finally, we indirectly assessed intestinal barrier integrity by evaluating the tight junction proteins ZO-1 and occludin levels (Fig. 11**a,** 11**b**). Western blot analysis did not reveal any significant decrease of tight junction proteins in the proximal colon of 10-month-old c-rel$^{-/-}$ mice, indirectly suggesting that the intestinal barrier integrity is preserved at this age**.**

4. Discussion

In the present study, we report a progressive accumulation of both α-syn and pSer-α-syn in myenteric plexus of the proximal colon of 2- and 10-months-old c-rel$^{-/-}$ mice, which is paralleled by α-syn accumulation in the DMV of 10-months-old c-rel$^{-/-}$ mice. These data, together with present and previous results showing intestinal constipation and α-syn deposition in the distal colon of 2-month-old c-rel$^{-/-}$ mice (Parrella et al.,

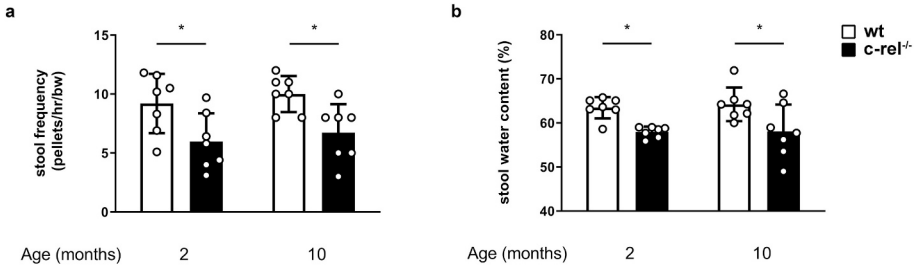

Fig. 10. c-rel$^{-/-}$ mice display reduced colon motility. Colon motility was investigated in 2- and 10-month-old wt and c-rel$^{-/-}$ male mice by measuring stool frequency (**a**) and stool water content (**b**) through the one-hour stool collection assay. (**a**) Stool frequency normalized for 30 g of body weight (bw). (**b**) Stool water %. $n = 7$ animals per group. Both the parameters were significantly reduced in 2- and 10-month-old c-rel$^{-/-}$ mice. Results are presented as mean ± SD. *$p < 0.05$, $\eta_p^2 = 0.378$, 95 % CI [0.352, 6.105] and [0.409, 6.162], two-way ANOVA followed by Sidak's multiple comparison test in **a**. *$p < 0.05$, $\eta_p^2 = 0.402$, 95 % CI [0.630, 10.430] and [1.241, 11.040], two-way ANOVA followed by Sidak's multiple comparison test in **b**.

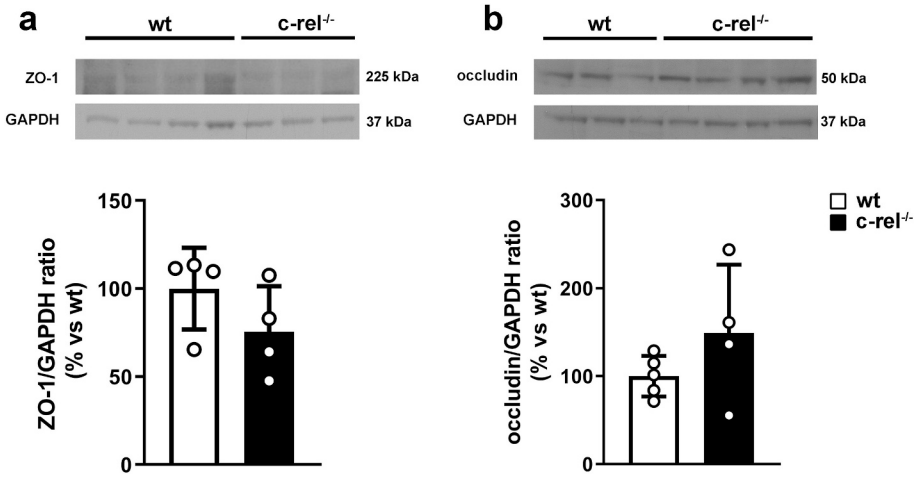

Fig. 11. c-rel$^{-/-}$ mice did not exhibit intestinal barrier alteration. Evaluation of the expression of tight junction proteins ZO-1 (**a**) and occluding (**b**) was performed in total protein extracts from proximal colon of 10-month-old wt and c-rel$^{-/-}$ male mice. Quantitative analysis of ZO-1 and occludin did not reveal any significant difference between wt and c-rel$^{-/-}$ male mice. $n = 4$ animals per group in **a**. $n = 4$–5 animals per group in **b**. Results are presented as mean ± SD.

2019), suggest that the α-syn accumulation in ENS of c-rel$^{-/-}$ mice could begin before the appearance of α-syn in the brain and before the onset of motor symptoms. Interestingly, in another mouse model of PD (A53T α-syn mice) a similar pattern of pathology progression, consisting in early constipation and colonic accumulation of α-syn without concomitant CNS involvement has been described (Rota et al., 2019). Our data are in line with Braak's staging model and a body of evidence reporting the presence of α-syn fibrils in intestinal biopsies from healthy patients who were prone to develop PD later in life (Hilton et al., 2014).

To assess whether α-syn accumulation was associated with oxidative stress in the proximal colon of the c-rel$^{-/-}$ mice, we analyzed NADPH oxidase activity and 3-NT-modified proteins in gut extracts. The oxidative stress biomarkers were already detectable in the colon at 2 months of age and they markedly increased at 10 months. These findings are consistent with existing literature indicating that oxidative and nitrosative stress are closely associated with PD pathology, both in patients and in animal models. For instance, Keeney and colleagues reported that activation of neuronal and microglial NADPH oxidases significantly contributes to disease development, as demonstrated in human tissues and rotenone-induced rat models (Keeney et al., 2022). NADPH oxidase-mediated oxidative stress was also observed in the proximal colon of 6-hydroxydopamine rat model of PD (Garrido-Gil et al., 2018) and was found to promote α-syn expression and aggregation in paraquat-based cellular and animal models of PD (Cristóvão et al., 2012). Similarly, increased immunoreactivity of NADPH oxidase catalytic subunits has been observed directly in the brains of patients with PD, supporting the role of oxidative enzyme activation in disease progression (Belarbi et al., 2017). Regarding protein modifications induced by oxidative stress, Forsyth and colleagues documented elevated intestinal 3-NT staining in the sigmoid intestinal mucosa of newly diagnosed patients compared to healthy controls, suggesting early nitrosative stress in disease progression (Forsyth et al., 2011).

Members of NADPH-oxidase family are expressed all along the gastrointestinal tract, in the epithelium, fibroblasts and smooth muscle cells, but also in dendritic cells and professional phagocytes (Aviello and Knaus, 2017; Bedard and Krause, 2007). Therefore, the enhanced NADPH-oxidase activity in the intestinal tissue can be associated with the infiltration of immune cells occurring at 10 months of age. Actually, the analysis of cells positive for the pan-leukocyte marker CD45 revealed an increased number of immune cells in the proximal colon of 10-month-old c-rel$^{-/-}$ mice. This in line with the increased gene expression of *PTPRC* encoding the CD45 protein in colonic biopsies from PD patients when compared to those from healthy subjects (Houser et al., 2021). While flow cytometry analysis of the CD45-positive cell subpopulation in the lamina propria of c-rel$^{-/-}$ mice did not reach statistical significance, it revealed a trend consistent with the significant findings obtained through immunohistochemistry, possibly due to differences in methodological sensitivity. However, quantification of CD11b+Ly6G+ colonic neutrophils revealed a significant increase in 10-month-old c-rel$^{-/-}$ mice compared to wt littermates. Neutrophils act as a double-edged sword in intestinal inflammatory processes: they play a critical role in early pathogen clearance and tissue repair but can trigger harmful inflammation when dysregulated (Schwab et al., 2007; Jorch and Kubes, 2017; Phillipson and Kubes, 2019; Drury et al., 2021). Their functional impact thus largely depends on timing and recruitment to the inflammatory site. It is conceivable that the increase in neutrophils observed in c-rel$^{-/-}$ mice reflects a compensatory response to rising intestinal inflammation, aimed at promoting homeostasis (Zhou and Liu, 2017).

To investigate molecular mediators contributing to intestinal inflammation in c-rel$^{-/-}$ mice, we assessed cytokine expression and observed a significant increase in IL-6 mRNA levels in the proximal colon. *IL-6* promotes the proliferation and differentiation of lymphocytes into a pro-inflammatory type, worsening the gut inflammation (Atreya and Neurath, 2005). Recently, the link between intestinal *IL-6* expression and PD has been explored (Guo et al., 2020; Xiromerisiou et al., 2023). The ascending colon of PD patients have shown increased expression of pro-inflammatory cytokines including *IL-6* (Devos et al., 2013). The trend for the IL6 protein increase, despite the significant increase in IL-6 mRNA in the colon of c-rel$^{-/-}$ mice, may suggest a partial occurrence of a post-transcriptional regulatory mechanisms, such as mRNA sequestration or translational repression, as already observed in other inflammatory contexts (Neininger et al., 2002; Paschoud et al., 2006; Akira and Maeda, 2021). Several studies have demonstrated that IL-6 hysteresis might result from the difference in complexity between creating a mature mRNA and a functional secretory protein. While a mature mRNA is produced in a relatively compact process, the synthesis of a protein is a multi-step pathway that requires time for its maturation and localization, including post-translational modifications and intracellular transport (Jena, 2008; Liang et al., 2015).

The *IL-17A* expression showed only a trend to increase in the colon of 10-month-old mice, leaving open the possibility that a further up regulation could progress only in later phases. Increased expression of *IL-17A* has been observed in both intestinal and brain tissues of PD patients, highlighting its involvement in mucosal inflammation and immune activation (Xiromerisiou et al., 2023; Perez-Pardo et al., 2019).

Despite the mild cytokine expression, starting from 10-13 months of age, c-rel$^{-/-}$ mice exhibited a colon shortening which serves as a hallmark of inflammatory processes in intestinal diseases. Previous studies, such

as those by Okayasu et al. (1990) and Yomogida et al. (2009), have demonstrated that colon shortening is a morphological change that correlates with the severity and chronicity of inflammation in colitis models. It is associated with the tissue remodelling of gastrointestinal tract in patients affected by ulcerative colitis and Chron's disease.

Multispectral Optoacoustic Tomography (MSOT) analysis was also performed in the colon of 10-months-old c-rel$^{-/-}$ mice. Being a non-invasive technique able to provide real-time insights into tissue oxygenation, hemoglobin levels and vascular changes, MSOT allows the detection of parameters indicative of inflammatory processes. The MSOT data revealed higher levels of HbO_2 in the colon compared to wt mice, as detected in the more typical inflammatory bowel diseases (Bhutiani et al., 2017).

Taken together, our data demonstrate that c-rel$^{-/-}$ mice are prone to develop a low-grade inflammatory state in the proximal colon. The deletion of NF-κB/c-Rel leads to the spontaneous development of early and progressive intestinal pathology, likewise that observed in PD patients, that correlates with the gut constipation detected from 2 months onward (Parrella et al., 2019).

Several factors have been proposed to contribute to altered colon motility and consequently to constipation in PD, including α-syn accumulation-mediated degeneration of the ENS, gut neurotransmitter imbalance, and gut microbiota dysbiosis (Xu et al., 2022). The loss of TH-positive neurons and the low-grade inflammatory state in the proximal colon of c-rel$^{-/-}$ mice support a potential link between these mechanisms and constipation.

The order in which oxidative stress, the inflammatory response and α-syn accumulation occur and interact in the gut remains to be elucidated yet. Though, it has been reported that α-syn accumulation, inflammation and oxidative stress circularly regulate and sustain one another (Kelly et al., 2014; Forsyth et al., 2011; Devos et al., 2013). Evidence from preclinical models demonstrates that gut inflammation together with a pro-oxidant state promote the accumulation of α-syn followed by its aggregation (Kelly et al., 2014; Pan-Montojo et al., 2010; Pan-Montojo et al., 2012; Shults, 2006). This process can establish an auto-sustaining positive feedback loop that drives the spreading of pathological α-syn (Lema Tomé et al., 2013; Houser and Tansey, 2017).

How NF-κB/c-Rel deficiency can trigger the aforementioned loop in the gut may be attributed to the decreased expression of the NF-κB/c-Rel-dependent genes, UCP4, MnSOD, and Bcl-xL (Chen et al., 2000; Bernard et al., 2001; Pizzi et al., 2005; Sarnico et al., 2009; Ho et al., 2012; Lanzillotta et al., 2015), which are involved in mitochondrial homeostasis, ROS/RNS generation, and ROS/RNS scavenging, as already observed in SN of c-rel$^{-/-}$ mice (Parrella et al., 2019).

In line with evidence describing increased nitration and nitrosylation of proteins, including α-syn, in PD (Duda et al., 2000; Giasson et al., 2000; Yao et al., 2004; Chung et al., 2004), we detected a significant increase of 3-NT-modified proteins in proximal colon at 10 months, with a positive trend to significance at 2 months, in c-rel$^{-/-}$ mice. Reactive nitrogen species promote intracellular α-syn accumulation and aggregation (Hodara et al., 2004). Thus, it can be speculated that dysfunction of mitochondrial antioxidant system in c-rel$^{-/-}$ mice may contribute to enhance oxidative/nitrosative stress leading the α-syn pathology.

Of note, significant reduction of NF-κB/c-Rel DNA-binding activity was evident in both SN of *post-mortem* PD brains and PBMCs of PD patients (Porrini et al., 2023). By supporting a role for NF-κB/c-Rel dysregulation in PD pathophysiology, our results demonstrate that c-rel$^{-/-}$ mice recapitulate progressive PD-like pathology also in the proximal colon, closely reflecting the prodromal enteric manifestations observed in patients.

As a possible limitation of this study, it can be argued that c-rel$^{-/-}$ model represents a specific genetic knockout that may not fully capture the complexity or heterogeneity of idiopathic PD in humans, which involves multifactorial genetic, environmental, and aging-related components. This notwithstanding, the c-rel$^{-/-}$ model provides a robust and reproducible system for investigating the early involvement of the gastrointestinal tract in PD as well as the mechanisms driving α-syn accumulation within the enteric nervous system. Furthermore, given the rise of α-syn detected in the DMV of 5–7 month-old mice (Parrella et al., 2019), it presents a valuable template to explore the hypothesis of gut-originating, vagus-mediated α-syn propagation to the brain, a concept with profound implications for early diagnosis, disease staging, and therapeutic intervention. By capturing both the temporal and anatomical aspects of gut involvement, the c-rel$^{-/-}$ model stands out as a powerful tool to advance translational research in PD and inform strategies for intercepting disease progression at its potential point of origin.

Supplementary data to this article can be found online at https://doi.org/10.1016/j.nbd.2025.107182.

CRediT authorship contribution statement

Edoardo Parrella: Writing – original draft, Investigation, Formal analysis, Conceptualization. **Michele Mario Gennari:** Writing – review & editing, Investigation, Formal analysis, Conceptualization. **Giulia Abate:** Writing – review & editing, Investigation, Formal analysis, Conceptualization. **Mariachiara Pucci:** Writing – review & editing, Investigation, Formal analysis, Conceptualization. **Tiziana Schioppa:** Investigation, Formal analysis, Conceptualization. **Daniela Bosisio:** Investigation, Formal analysis, Conceptualization. **Emanuela Tirelli:** Investigation, Formal analysis. **Marina Benarese:** Investigation, Formal analysis. **Gaia Vegezzi:** Conceptualization. **Maria Grazia Silletti:** Investigation, Formal analysis. **Chiara Fritzsch:** Investigation, Formal analysis. **Daniela Uberti:** Writing – review & editing, Investigation, Formal analysis, Conceptualization. **Marina Pizzi:** Writing – review & editing, Supervision, Investigation, Funding acquisition, Formal analysis, Conceptualization. **Vanessa Porrini:** Writing – review & editing, Supervision, Investigation, Funding acquisition, Formal analysis, Conceptualization.

Declaration of generative AI and AI-assisted technologies in the writing process

During the preparation of this work the authors used the AI-tool ChatGPT (version GPT-4o) in order to improve language and readability of the text. After using this tool, the authors reviewed and edited the content as needed and take full responsibility for the content of the publication.

Funding

This work was supported by the Italian Ministry of Universities and Research PON Programme (Grant n° ARS01_01226) and by Fondazione Cariplo (Grant n° 2018–0391).

Declaration of competing interest

The authors declare the following financial interests/personal relationships which may be considered as potential competing interests:

Marina Pizzi reports financial support was provided by Italian Ministry of Universities. Vanessa Porrini reports financial support was provided by Fondazione Cariplo. If there are other authors, they declare that they have no known competing financial interests or personal relationships that could have appeared to influence the work reported in this paper.

Acknowledgements

This research was funded by the Italian Ministry of University and Research PON Programme, grant n° ARS01_01226 and by Fondazione Cariplo, grant n° 2018-0391. The authors performed experiments at the Imaging Platform and Flow Cytometry Platform of the Department of Molecular and Translational Medicine of the University of Brescia. We

are thankful to Dr. Thomas Sardella for the assistance in the MSOT experiment and analysis.

Data availability

All data generated and/or analyzed during the current study are available from the corresponding author on reasonable request.

References

Abbott, R.D., Petrovitch, H., White, L.R., Masaki, K.H., Tanner, C.M., Curb, J.D., Grandinetti, A., Blanchette, P.L., Popper, J.S., Ross, G.W., 2002. Frequency of bowel movements and future risk of Parkinson's disease. Neurology 58 (5), 838–839. https://doi.org/10.1212/WNL.58.5.838-a.

Akira, S., Maeda, K., 2021. Control of RNA stability in immunity. Annu. Rev. Immunol. 39 (1), 481–509. https://doi.org/10.1146/annurev-immunol-101819-075147.

Aldecoa, I., Navarro-Otano, J., Stefanova, N., Sprenger, F.S., Seppi, K., Poewe, W., Cuatrecasas, M., Valldeoriola, F., Gelpi, E., Tolosa, E., 2015. Alpha-synuclein immunoreactivity patterns in the enteric nervous system. Neurosci. Lett. 602, 145–149. https://doi.org/10.1016/j.neulet.2015.07.005.

Atreya, R., Neurath, M.F., 2005. Involvement of IL-6 in the pathogenesis of inflammatory bowel disease and colon cancer. Clin. Rev. Allergy Immunol. 28 (3), 187–195. https://doi.org/10.1385/CRIAI:28:3:187.

Aviello, G., Knaus, U.G., 2017. ROS in gastrointestinal inflammation: rescue or sabotage? Br. J. Pharmacol. 174 (12), 1704–1718. https://doi.org/10.1111/bph.13428.

Baiguera, C., Alghisi, M., Pinna, A., Bellucci, A., De Luca, M.A., Frau, L., Morelli, M., Ingrassia, R., Benarese, M., Porrini, V., et al., 2012. Late-onset parkinsonism in NFκB/c-Rel-deficient mice. Brain 135 (9), 2750–2765. https://doi.org/10.1093/brain/aws193.

Balestrino, R., Schapira, A.H.V., 2020. Parkinson disease. Eur. J. Neurol. 27 (1), 27–42. https://doi.org/10.1111/ene.14108.

Beckman, J.S., 1996. Oxidative damage and tyrosine nitration from peroxynitrite. Chem. Res. Toxicol. 9 (5), 836–844. https://doi.org/10.1021/tx9501445.

Bedard, K., Krause, K.H., 2007. The NOX family of ROS-generating NADPH oxidases: physiology and pathophysiology. Physiol. Rev. 87 (1), 245–313. https://doi.org/10.1152/physrev.00044.2005.

Belarbi, K., Cuvelier, E., Destée, A., Gressier, B., Chartier-Harlin, M.C., 2017. NADPH oxidases in Parkinson's disease: a systematic review. Mol. Neurodegener. 12, 1–18. https://doi.org/10.1186/s13024-017-0225-5.

Bellucci, A., Bubacco, L., Longhena, F., Parrella, E., Faustini, G., Porrini, V., Bono, F., Missale, C., Pizzi, M., 2020. Nuclear factor-κB dysregulation and α-syn pathology: critical interplay in the pathogenesis of Parkinson's disease. Front. Aging Neurosci. 12. https://doi.org/10.3389/fnagi.2020.00068. Article 68.

Ben-Shlomo, Y., Darweesh, S., Llibre-Guerra, J., Marras, C., San Luciano, M., Tanner, C., 2024. The epidemiology of Parkinson's disease. Lancet 403 (10423), 283–292. https://doi.org/10.1016/S0140-6736(23)01419-8.

Bernard, D., Quatannens, B., Begue, A., Vandenbunder, B., Abbadie, C., 2001. Antiproliferative and antiapoptotic effects of crel may occur within the same cells via the up-regulation of manganese superoxide dismutase. Cancer Res. 61 (6), 2656–2664.

Berthoud, H.-R., Neuhuber, W.L., 2000. Functional and chemical anatomy of the afferent vagal system. Auto. Neurosci. Basic Clin. 85 (1–3), 98–101. https://doi.org/10.1016/S1566-0702(00)00227-7.

Berthoud, H.R., Carlson, N.R., Powley, T.L., 1991. Topography of efferent vagal innervation of the rat gastrointestinal tract. Am. J. Phys. Regul. Integr. Comp. Phys. 260 (1), R200–R207. https://doi.org/10.1152/ajpregu.1991.260.1.r200.

Bhutiani, N., Grizzle, W.E., Galandiuk, S., Otali, D., Dryden, G.W., Egilmez, N.K., McNally, L.R., 2017. Noninvasive imaging of colitis using multispectral optoacoustic tomography. J. Nucl. Med. 58 (6), 1009–1012. https://doi.org/10.2967/jnumed.116.184705.

Böttner, M., Zorenkov, D., Hellwig, I., Barrenschee, M., Harde, J., Fricke, T., Deuschl, G., Egberts, J.H., Becker, T., Fritscher-Ravens, A., et al., 2012. Expression pattern and localization of alpha-synuclein in the human enteric nervous system. Neurobiol. Dis. 48 (3), 474–480. https://doi.org/10.1016/j.nbd.2012.07.018.

Braak, H., Rüb, U., Gai, W.P., Del Tredici, K., 2003. Idiopathic Parkinson's disease: possible routes by which vulnerable neuronal types may be subject to neuroinvasion by an unknown pathogen. J. Neural Transm. 110 (5), 517–536. https://doi.org/10.1007/s00702-002-0808-2.

Braak, H., de Vos, R.A.I., Bohl, J., Del Tredici, K., 2006. Gastric α-syn immunoreactive inclusions in Meissner's and Auerbach's plexuses in cases staged for Parkinson's disease-related brain pathology. Neurosci. Lett. 396 (1), 67–72. https://doi.org/10.1016/j.neulet.2005.11.012.

Chen, C., Edelstein, L.C., Gélinas, C., 2000. The Rel/NF-κB family directly activates expression of the apoptosis inhibitor Bcl-xL. Mol. Cell. Biol. 20 (8), 2687–2695. https://doi.org/10.1128/MCB.20.8.2687-2695.2000.

Chen, H., Zhao, E.J., Zhang, W., Lu, Y., Liu, R., Huang, X., Ciesielski-Jones, A.J., Justice, M.A., Cousins, D.S., Peddada, S., 2015. Meta-analyses on prevalence of selected Parkinson's nonmotor symptoms before and after diagnosis. Transl. Neurodegener. 4. https://doi.org/10.1186/2047-9158-4-1. Article 1.

Chung, K.K., Thomas, B., Li, X., Pletnikova, O., Troncoso, J.C., Marsh, L., Dawson, T.M., 2004. S-nitrosylation of parkin regulates ubiquitination and compromises parkin's protective function. Science 304 (5675), 1328–1331. https://doi.org/10.1126/science.1093891.

Costa, H.N., Esteves, A.R., Empadinhas, N., Cardoso, S.M., 2023. Parkinson's disease: a multisystem disorder. Neurosci. Bull. 39 (1), 113–124. https://doi.org/10.1007/s12264-022-00934-6.

Cristóvão, A.C., Guhathakurta, S., Bok, E., Je, G., Yoo, S.D., Choi, D.H., Kim, Y.S., 2012. NADPH oxidase 1 mediates α-synucleinopathy in Parkinson's disease. J. Neurosci. 32 (42), 14465–14477. https://doi.org/10.1523/JNEUROSCI.2246-12.2012.

Devos, D., Lebouvier, T., Lardeux, B., Biraud, M., Rouaud, T., Pouclet, H., Coron, E., Bruley Des Varannes, S., Naveilhan, P., Nguyen, J.-M., et al., 2013. Colonic inflammation in Parkinson's disease. Neurobiol. Dis. 50, 42–48. https://doi.org/10.1016/j.nbd.2012.09.007.

Dogra, N., Mani, R.J., Katare, D.P., 2022. The gut-brain axis: two ways signaling in Parkinson's disease. Cell. Mol. Neurobiol. 42 (2), 315–332. https://doi.org/10.1007/s10571-021-01066-7.

Dovonou, A., Bolduc, C., Soto Linan, V., Gora, C., Peralta Iii, M.R., Lévesque, M., 2023. Animal models of Parkinson's disease: bridging the gap between disease hallmarks and research questions. Transl. Neurodegener. 12 (1), 36. https://doi.org/10.1186/s40035-023-00368-8.

Drury, B., Hardisty, G., Gray, R.D., Ho, G.T., 2021. Neutrophil extracellular traps in inflammatory bowel disease: pathogenic mechanisms and clinical translation. Cell. Mol. Gastroenterol. Hepatol. 12 (1), 321–333. https://doi.org/10.1016/j.jcmgh.2021.03.002.

Duda, J.E., Giasson, B.I., Chen, Q., Gur, T.L., Hurtig, H.I., Stern, M.B., Trojanowski, J.Q., 2000. Widespread nitration of pathological inclusions in neurodegenerative synucleinopathies. Am. J. Pathol. 157 (5), 1439–1445. https://doi.org/10.1016/S0002-9440(10)64781-5.

Faustini, G., Bono, F., Valerio, A., Pizzi, M., Spano, P., Bellucci, A., 2017. Mitochondria and α-synuclein: friends or foes in the pathogenesis of Parkinson's disease? Genes 8 (12). https://doi.org/10.3390/genes8120377. Article 377.

Fitzgerald, E., Murphy, S., Martinson, H.A., 2019. Alpha-synuclein pathology and the role of the microbiota in Parkinson's disease. Front. Neurosci. 13. https://doi.org/10.3389/fnins.2019.00369. Article 369.

Forsyth, C.B., Shannon, K.M., Kordower, J.H., Voigt, R.M., Shaikh, M., Jaglin, J.A., Estes, J.D., Dodiya, H.B., Keshavarzian, A., 2011. Increased intestinal permeability correlates with sigmoid mucosa alpha-synuclein staining and endotoxin exposure markers in early Parkinson's disease. PLoS One 6 (12). https://doi.org/10.1371/journal.pone.0028032. Article e28032.

France, M., Bhattarai, Y., Galligan, J.J., Xu, H., 2012. Impaired propulsive motility in the distal but not proximal colon of BK channel β1-subunit knockout mice. Neurogastroenterol. Motil. 24 (10), e450–e459. https://doi.org/10.1111/j.1365-2982.2012.01981.x.

Fujino, S., Andoh, A., Bamba, S., Ogawa, A., Hata, K., Araki, Y., Bamba, T., Fujiyama, Y., 2003. Increased expression of interleukin 17 in inflammatory bowel disease. Gut 52 (1), 65–70. https://doi.org/10.1136/gut.52.1.65.

Garrido-Gil, P., Rodriguez-Perez, A., Dominguez-Meijide, A., Guerra, M.J., Labandeira-Garcia, J.L., 2018. Bidirectional neural interaction between central dopaminergic and gut lesions in Parkinson's disease models. Mol. Neurobiol. 55 (9), 7297–7316. https://doi.org/10.1007/s12035-018-0937-8.

Giasson, B.I., Duda, J.E., Murray, I.V., Chen, Q., Souza, J.M., Hurtig, H.I., Lee, Y., V. M., 2000. Oxidative damage linked to neurodegeneration by selective α-synuclein nitration in synucleinopathy lesions. Science 290 (5493), 985–989. https://doi.org/10.1126/science.290.5493.985.

Gilmore, T.D., Wolenski, F.S., 2012. NF-κB: where did it come from and why? Immunol. Rev. 246 (1), 14–35. https://doi.org/10.1111/j.1600-065X.2012.01096.x.

Gold, A., Turkalp, Z.T., Munoz, D.G., 2013. Enteric alpha-synuclein expression is increased in Parkinson's disease but not Alzheimer's disease. Mov. Disord. 28 (2), 237–241. https://doi.org/10.1002/mds.25298.

Gonella, J., Bouvier, M., Blanquet, F., 1987. Extrinsic nervous control of motility of small and large intestines and related sphincters. Physiol. Rev. 67 (3), 902–961. https://doi.org/10.1152/physrev.1987.67.3.902.

Guo, Y., Wang, B., Wang, T., Gao, L., Yang, Z.J., Wang, F.F., Shang, H.W., Hua, R., Xu, J. D., 2020. Biological characteristics of IL-6 and related intestinal diseases. Int. J. Biol. Sci. 17 (1), 204–219. https://doi.org/10.7150/ijbs.51362.

Hawkes, C.H., Del Tredici, K., Braak, H., 2007. Parkinson's disease: a dual-hit hypothesis. Neuropathol. Appl. Neurobiol. 33 (6), 599–614. https://doi.org/10.1111/j.1365-2990.2007.00874.x.

Hilton, D., Stephens, M., Kirk, L., Edwards, P., Potter, R., Zajicek, J., Broughton, E., Hagan, H., Carroll, C., 2014. Accumulation of α-syn in the bowel of patients in the pre-clinical phase of Parkinson's disease. Acta Neuropathol. 127 (2), 235–241. https://doi.org/10.1007/s00401-013-1214-6.

Ho, J.W.M., Ho, P.W.L., Liu, H.F., So, D.H.F., Chan, K.H., Tse, Z.H.M., Ho, S.L., 2012. UCP4 is a target effector of the NF-κB c-Rel prosurvival pathway against oxidative stress. Free Radic. Biol. Med. 53 (2), 383–394. https://doi.org/10.1016/j.freeradbiomed.2012.05.002.

Hodara, R., Norris, E.H., Giasson, B.I., Mishizen-Eberz, A.J., Lynch, D.R., Lee, V.M.Y., Ischiropoulos, H., 2004. Functional consequences of α-synuclein tyrosine nitration: diminished binding to lipid vesicles and increased fibril formation. J. Biol. Chem. 279 (46), 47746–47753. https://doi.org/10.1074/jbc.M408906200.

Houser, M.C., Caudle, W.M., Chang, J., Kannarkat, G.T., Yang, Y., Kelly, S.D., Oliver, D., Joers, V., Shannon, K.M., Keshavarzian, A., Tansey, M.G., 2021. Experimental colitis promotes sustained, sex-dependent, T-cell-associated neuroinflammation and parkinsonian neuropathology. Acta Neuropathol. Commun. 9 (1). https://doi.org/10.1186/s40478-021-01240-4. Article 139.

Houser, M.C., Tansey, M.G., 2017. The gut-brain axis: is intestinal inflammation a silent driver of Parkinson's disease pathogenesis? NPJ Parkinson's dis. 3 (1), 3. https://doi.org/10.1038/s41531-016-0002-0.

Jena, B.P., 2008. Porosome: the universal molecular machinery for cell secretion. Mol. Cell 26 (6), 517–529. https://doi.org/10.1016/S1016-8478(23)14032-5.
Jiang, P., Dickson, D.W., 2018. Parkinson's disease: experimental models and reality. Acta Neuropathol. 135 (1), 13–32. https://doi.org/10.1007/s00401-017-1788-5.
Jin, B.R., Chung, K.-S., Cheon, S.-Y., Lee, M., Hwang, S., Noh Hwang, S., Rhee, K.-J., An, H.-J., 2017. Rosmarinic acid suppresses colonic inflammation in dextran sulphate sodium (DSS)-induced mice via dual inhibition of NF-κB and STAT3 activation. Sci. Rep. 7. https://doi.org/10.1038/srep46252. Article 46252.
Jorch, S.K., Kubes, P., 2017. An emerging role for neutrophil extracellular traps in noninfectious disease. Nat. Med. 23 (3), 279–287. https://doi.org/10.1038/nm.4294.
Kalia, L.V., Lang, A.E., 2015. Parkinson's disease. Lancet 386 (9996), 896–912. https://doi.org/10.1016/S0140-6736(14)61393-3.
Keeney, M.T., Hoffman, E.K., Farmer, K., Bodle, C.R., Fazzari, M., Zharikov, A., Di Maio, R., 2022. NADPH oxidase 2 activity in Parkinson's disease. Neurobiol. Dis. 170, 105754. https://doi.org/10.1016/j.nbd.2022.105754.
Kelly, L.P., Carvey, P.M., Keshavarzian, A., Shannon, K.M., Shaikh, M., Bakay, R.A.E., Kordower, J.H., 2014. Progression of intestinal permeability changes and alpha-synuclein expression in a mouse model of Parkinson's disease. Mov. Disord. 29 (8), 999–1009. https://doi.org/10.1002/mds.25736.
Lal, R., Chopra, K., 2024. Experimental models of Parkinson's disease: challenges and opportunities. Eur. J. Pharmacol. 980, 176819. https://doi.org/10.1016/j.ejphar.2024.176819.
Lanzillotta, A., Porrini, V., Bellucci, A., Benarese, M., Branca, C., Parrella, E., Spano, P.F., Pizzi, M., 2015. NF-κB in innate neuroprotection and age-related neurodegenerative diseases. Front. Neurol. 6. https://doi.org/10.3389/fneur.2015.00098. Article 98.
Lema Tomé, C.M., Tyson, T., Rey, N.L., Grathwohl, S., Britschgi, M., Brundin, P., 2013. Inflammation and α-synuclein's prion-like behavior in Parkinson's disease—is there a link? Mol. Neurobiol. 47 (2), 561–574. https://doi.org/10.1007/s12035-012-8267-8.
Liang, X., Liu, Y., Mei, S., Zhang, M., Xin, J., Zhang, Y., Yang, R., 2015. MicroRNA-22 impairs anti-tumor ability of dendritic cells by targeting p38. PLoS One 10 (3), e0121510. https://doi.org/10.1371/journal.pone.0121510.
Liou, H.-C., Jin, Z., Tumang, J., Andjelic, S., Smith, K.A., Liou, M.-L., 1999. C-Rel is crucial for lymphocyte proliferation but dispensable for T cell effector function. Int. Immunol. 11 (3), 361–371. https://doi.org/10.1093/intimm/11.3.361.
Longhena, F., Faustini, G., Spillantini, M.G., Bellucci, A., 2019. Living in promiscuity: the multiple partners of alpha-synuclein at the synapse in physiology and pathology. Int. J. Mol. Sci. 20 (1). https://doi.org/10.3390/ijms20010141. Article 141.
Matsunaga, H., Hokari, R., Higashiyama, M., Kurihara, C., Okada, Y., Watanabe, C., Komoto, S., Nakamura, M., Kawaguchi, A., Nagao, S., et al., 2009. Roles of intestinal epithelial cells in the maintenance of gut homeostasis with respect to segmental differences between the proximal and distal colon in inflammatory bowel disease. J. Crohn's Colitis 3 (1), S25. https://doi.org/10.1016/S1873-9946(09)60097-6.
Micheau, A., Hoa, D., 2018. Labeled cross-sectional anatomy of the mouse on micro-CT. Vet. Anat. https://doi.org/10.37019/vet-anatomy/564757.
Mota, M., Porrini, V., Parrella, E., Benarese, M., Bellucci, A., Rhein, S., Schwaninger, M., Pizzi, M., 2020. Neuroprotective epi-drugs quench the inflammatory response and microglial/macrophage activation in a mouse model of permanent brain ischemia. J. Neuroinflammation 17 (1). https://doi.org/10.1186/s12974-020-02028-4. Article 316.
Neininger, A., Kontoyiannis, D., Kotlyarov, A., Winzen, R., Eckert, R., Volk, H.D., Gaestel, M., 2002. MK2 targets AU-rich elements and regulates biosynthesis of tumor necrosis factor and interleukin-6 independently at different post-transcriptional levels. J. Biol. Chem. 277 (5), 3065–3068. https://doi.org/10.1074/jbc.C100685200.
Okayasu, I., Hatakeyama, S., Yamada, M., Ohkusa, T., Inagaki, Y., Nakaya, R., 1990. A novel method in the induction of reliable experimental acute and chronic ulcerative colitis in mice. Gastroenterology 98 (3), 694–702. https://doi.org/10.1016/0016-5085(90)90290-H.
Pan-Montojo, F., Anichtchik, O., Dening, Y., Knels, L., Pursche, S., Jung, R., Jackson, S., Gille, G., Spillantini, M.G., Reichmann, H., et al., 2010. Progression of Parkinson's disease pathology is reproduced by intragastric administration of rotenone in mice. PLoS One 5 (1). https://doi.org/10.1371/journal.pone.0008762. Article e8762.
Pan-Montojo, F., Schwarz, M., Winkler, C., Arnhold, M., O'Sullivan, G.A., Pal, A., Said, J., Marsico, G., Verbavatz, J.M., Rodrigo-Angulo, M., et al., 2012. Environmental toxins trigger PD-like progression via increased alpha-synuclein release from enteric neurons in mice. Sci. Rep. 2. https://doi.org/10.1038/srep00898. Article 898.
Parrella, E., Bellucci, A., Porrini, V., Benarese, M., Lanzillotta, A., Faustini, G., Longhena, F., Abate, G., Uberti, D., Pizzi, M., 2019. NF-κB/c-Rel deficiency causes Parkinson's disease-like prodromal symptoms and progressive pathology in mice. Transl. Neurodegener. 8. https://doi.org/10.1186/s40035-019-0154-z. Article 16.
Parrella, E., Del Gallo, F., Porrini, V., Gussago, C., Benarese, M., Fabene, P.F., Pizzi, M., 2022. Age-dependent neuropsychiatric symptoms in the NF-κB/c-Rel knockout mouse model of Parkinson's disease. Front. Behav. Neurosci. 16. https://doi.org/10.3389/fnbeh.2022.831664. Article 831664.
Parrella, E., Porrini, V., Gennari, M.M., Benarese, M., Gallo, F.D., Andrioli, A., Fritzsch, C., Bentivoglio, M., Fabene, P.F., Pizzi, M., 2025. Sex-related differences in phenotype and nigro-striatal degeneration of c-rel−/−mouse model of Parkinson's disease. Biol. Sex Differ. 16 (1), 1–16. https://doi.org/10.1186/s13293-025-00761-0.
Paschoud, S., Dogar, A.M., Kuntz, C., Grisoni-Neupert, B., Richman, L., Kühn, L.C., 2006. Destabilization of interleukin-6 mRNA requires a putative RNA stem-loop structure, an AU-rich element, and the RNA-binding protein AUF1. Mol. Cell. Biol. https://doi.org/10.1128/MCB.01155-06.
Perez-Pardo, P., Dodiya, H.B., Engen, P.A., Forsyth, C.B., Huschens, A.M., Shaikh, M., Keshavarzian, A., 2019. Role of TLR4 in the gut-brain axis in Parkinson's disease: a translational study from men to mice. Gut 68 (5), 829–843. https://doi.org/10.1136/gutjnl-2018-316844.
Perez-Pardo, P., Kliest, T., Dodiya, H.B., Broersen, L.M., Garssen, J., Keshavarzian, A., Kraneveld, A.D., 2017. The gut-brain axis in Parkinson's disease: possibilities for food-based therapies. Eur. J. Pharmacol. 817, 86–95. https://doi.org/10.1016/j.ejphar.2017.05.042.
Phillips, R.J., Walter, G.C., Wilder, S.L., Baronowsky, E.A., Powley, T.L., 2008. Alpha-synuclein-immunopositive myenteric neurons and vagal preganglionic terminals: autonomic pathway implicated in Parkinson's disease? Neuroscience 153 (3), 733–750. https://doi.org/10.1016/j.neuroscience.2008.02.074.
Phillipson, M., Kubes, P., 2019. The healing power of neutrophils. Trends Immunol. 40 (7), 635–647. https://doi.org/10.1016/j.it.2019.05.001.
Pizzi, M., Sarnico, I., Boroni, F., Benarese, M., Steimberg, N., Mazzoleni, G., Spano, P.F., 2005. NF-κB factor c-Rel mediates neuroprotection elicited by mGlu5 receptor agonists against amyloid β-peptide toxicity. Cell Death Differ. 12 (7), 761–772. https://doi.org/10.1038/sj.cdd.4401598.
Poewe, W., Seppi, K., Tanner, C.M., Halliday, G.M., Brundin, P., Volkmann, J., Schrag, A.E., Lang, A.E., 2017. Parkinson disease. Nat. Rev. Dis. Prim. 3. https://doi.org/10.1038/nrdp.2017.13. Article 17013.
Poles, M.Z., Bódi, N., Bagyánszki, M., Fekete, É., Mészáros, A.T., Varga, G., Szűcs, S., Nászai, A., Kiss, L., Kozlov, A.V., Boros, M., Kaszaki, J., 2018. Reduction of nitrosative stress by methane: neuroprotection through xanthine oxidoreductase inhibition in a rat model of mesenteric ischemia-reperfusion. Free Radic. Biol. Med. 120, 160–169. https://doi.org/10.1016/j.freeradbiomed.2018.03.024.
Porrini, V., Mota, M., Parrella, E., Bellucci, A., Benarese, M., Faggi, L., Tonin, P., Spano, P.F., Pizzi, M., 2017. Mild inflammatory profile without gliosis in the c-Rel deficient mouse modeling a late-onset parkinsonism. Front. Aging Neurosci. 9. https://doi.org/10.3389/fnagi.2017.00229. Article 229.
Porrini, V., Pilotto, A., Vezzoli, M., Lanzillotta, A., Gennari, M.M., Bonacina, S., Alberici, A., Turrone, R., Bellucci, A., Antonini, A., et al., 2023. NF-κB/c-Rel DNA-binding is reduced in substantia nigra and peripheral blood mononuclear cells of Parkinson's disease patients. Neurobiol. Dis. 180. https://doi.org/10.1016/j.nbd.2023.106067. Article 106067.
Postuma, R.B., Gagnon, J.F., Pelletier, A., Montplaisir, J., 2013. Prodromal autonomic symptoms and signs in Parkinson's disease and dementia with Lewy bodies. Mov. Disord. 28 (5), 597–604. https://doi.org/10.1002/mds.25445.
Pucci, M., Aria, F., Premoli, M., Maccarinelli, G., Mastinu, A., Bonini, S., Memo, M., Uberti, D., Abate, G., 2021. Methylglyoxal affects cognitive behaviour and modulates RAGE and presenilin-1 expression in hippocampus of aged mice. Food Chem. Toxicol. 158. https://doi.org/10.1016/j.fct.2021.112608. Article 112608.
Pucci, M., Mandrone, M., Chiocchio, I., Sweeney, E.M., Tirelli, E., Uberti, D., Memo, M., Poli, F., Mastinu, A., Abate, G., 2022. Different seasonal collections of Ficus carica L. leaves diversely modulate lipid metabolism and adipogenesis in 3T3-L1 adipocytes. Nutrients 14 (14). https://doi.org/10.3390/nu14142833. Article 2833.
Rota, L., Pellegrini, C., Benvenuti, L., Antonioli, L., Fornai, M., Blandizzi, C., Cattaneo, A., Colla, E., 2019. Constipation, deficit in colon contractions and alpha-synuclein inclusions within the colon precede motor abnormalities and neurodegeneration in the central nervous system in a mouse model of alpha-synucleinopathy. Transl. Neurodegener. 8. https://doi.org/10.1186/s40035-019-0146-z. Article 5.
Sarnico, I., Branca, C., Lanzillotta, A., Porrini, V., Benarese, M., Spano, P.F., Pizzi, M., 2012. NF-κB and epigenetic mechanisms as integrative regulators of brain resilience to anoxic stress. Brain Res. 1476, 203–210. https://doi.org/10.1016/j.brainres.2012.04.013.
Sarnico, I., Lanzillotta, A., Boroni, F., Benarese, M., Alghisi, M., Schwaninger, M., Pizzi, M., 2009. NF-κB p50/RelA and c-Rel-containing dimers: opposite regulators of neuron vulnerability to ischaemia. J. Neurochem. 108 (2), 475–485. https://doi.org/10.1111/j.1471-4159.2008.05783.x.
Savica, R., Carlin, J.M., Grossardt, B.R., Bower, J.H., Ahlskog, J.E., Maraganore, D.M., Bharucha, A.E., Rocca, W.A., 2009. Medical records documentation of constipation preceding Parkinson disease: a case-control study. Neurology 73 (21), 1752–1758. https://doi.org/10.1212/WNL.0b013e3181c34af5.
Schwab, J.M., Chiang, N., Arita, M., Serhan, C.N., 2007. Resolvin E1 and protectin D1 activate inflammation-resolution programmes. Nature 447 (7146), 869–874. https://doi.org/10.1038/nature05877.
Shannon, K.M., Keshavarzian, A., Dodiya, H.B., Jakate, S., Kordower, J.H., 2012a. Is alpha-synuclein in the colon a biomarker for premotor Parkinson's disease? Evidence from 3 cases. Mov. Disord. 27 (6), 716–719. https://doi.org/10.1002/mds.25020.
Shannon, K.M., Keshavarzian, A., Mutlu, E., Dodiya, H.B., Daian, D., Jaglin, J.A., Kordower, J.H., 2012b. Alpha-synuclein in colonic submucosa in early untreated Parkinson's disease. Mov. Disord. 27 (6), 709–715. https://doi.org/10.1002/mds.23838.
Shults, C.W., 2006. Lewy bodies. Proc. Natl. Acad. Sci. 103 (6), 1661–1668. https://doi.org/10.1073/pnas.0509567103.
Stokholm, M.G., Danielsen, E.H., Hamilton-Dutoit, S.J., Borghammer, P., 2016. Pathological α-syn in gastrointestinal tissues from prodromal Parkinson disease patients. Ann. Neurol. 79 (6), 940–949. https://doi.org/10.1002/ana.24648.
Szabo, R., Callies, L.L.K., Bugge, T.H., 2019. Matriptase drives early-onset intestinal failure in a mouse model of congenital tufting enteropathy. Development 146 (21). https://doi.org/10.1242/dev.183392. Article dev183392.
Wooten, G.F., Currie, L.J., Bovbjerg, V.E., Lee, J.K., Patrie, J., 2004. Are men at greater risk for Parkinson's disease than women? J. Neurol. Neurosurg. Psychiatry 75 (4), 637–639. https://doi.org/10.1136/jnnp.2003.020982.
Xiromerisiou, G., Marogianni, C., Androutsopoulou, A., Ntavaroukas, P., Mysiris, D., Papoutsopoulou, S., 2023. Parkinson's disease, it takes guts: the correlation between

intestinal microbiome and cytokine network with neurodegeneration. Biology 12 (1). https://doi.org/10.3390/biology12010093. Article 93.
Xu, Y., Hunt, N.H., Bao, S., 2008. The role of granulocyte macrophage-colony-stimulating factor in acute intestinal inflammation. Cell Res. 18 (12), 1220–1229. https://doi.org/10.1038/cr.2008.310.
Xu, J., Wang, L., Chen, X., Le, W., 2022. New understanding on the pathophysiology and treatment of constipation in Parkinson's disease. Front. Aging Neurosci. 14, 917499. https://doi.org/10.3389/fnagi.2022.917499.
Yao, D., Gu, Z., Nakamura, T., Shi, Z.Q., Ma, Y., Gaston, B., Lipton, S.A., 2004. Nitrosative stress linked to sporadic Parkinson's disease: S-nitrosylation of parkin regulates its E3 ubiquitin ligase activity. Proc. Natl. Acad. Sci. 101 (29), 10810–10814. https://doi.org/10.1073/pnas.0404161101.
Yomogida, S., Kojima, Y., Tsutsumi-Ishii, Y., Hua, J., Sakamoto, K., Nagaoka, I., 2009. Glucosamine, a naturally occurring amino monosaccharide, suppresses dextran sulfate sodium-induced colitis in rats. Int. J. Mol. Med. 23 (4), 521–527. https://doi.org/10.3892/ijmm_00000159.
Zhou, G.X., Liu, Z.J., 2017. Potential roles of neutrophils in regulating intestinal mucosal inflammation of inflammatory bowel disease. J. Dig. Dis. 18 (9), 495–503. https://doi.org/10.1111/1751-2980.12540.